

# Excimer Evolution Hampers Symmetry-Broken Charge Separated State

Ebin Sebastian<sup>‡</sup>, Jeswin Sunny<sup>‡</sup> and Mahesh Hariharan<sup>\*</sup>

School of Chemistry, Indian Institute of Science Education and Research Thiruvananthapuram (IISER TVM), Maruthamala P. O., Vithura, Thiruvananthapuram 695551, Kerala, India.

\*E-mail: mahesh@iisertvm.ac.in

## Electronic Supplementary Information (ESI)

### Table of Contents

<b>Section 1: Materials and Methods</b> .....	<b>5</b>
1.1 Computational Analysis .....	5
1.2 Time-Resolved Emission Spectra (TRES) Analysis .....	5
1.3 Electrochemistry .....	5
1.4 Weller Analysis .....	6
1.5 Femtosecond transient absorption (fsTA) measurement .....	6
1.6 Global Analysis .....	7
1.7 TheoDORE Analysis .....	7
<b>Section 2: Synthesis and Characterization</b> .....	<b>8</b>
<b>Scheme S1:</b> Showing the synthesis scheme for monomers ( <b>SPDI</b> and <b>NPDI</b> ) and dimers ( <b>SC-SPDI<sub>2</sub></b> and <b>SC-NPDI<sub>2</sub></b> ) .....	8
<b>Synthesis of NPDI:</b> .....	8
<b>Synthesis of SPDI:</b> .....	8
<b>Synthesis of SC-NPDI<sub>2</sub>:</b> .....	9
<b>Synthesis of SC-SPDI<sub>2</sub></b> .....	9
<b>Section 3: Tables</b> .....	<b>10</b>
<b>Table S1:</b> Oscillator strength for different transitions of <b>SPDI</b> calculated at TD- $\omega$ B97XD/ def2svp level of theory .....	10
<b>Table S2:</b> Oscillator strength for different transitions of <b>NPDI</b> calculated at TD- $\omega$ B97XD/ def2svp level of theory .....	10
<b>Table S3:</b> Oscillator strength for different transitions of <b>SC-SPDI<sub>2</sub></b> calculated at TD- $\omega$ B97XD/ def2svp level of theory .....	10
<b>Table S4:</b> Oscillator strength for different transitions of <b>SC-NPDI<sub>2</sub></b> calculated at TD- $\omega$ B97XD/ def2svp level of theory .....	11
<b>Table S5:</b> Summary of redox potentials and HOMO/LUMO calculations of <b>SC-SPDI<sub>2</sub></b> and <b>SC-NPDI<sub>2</sub></b> (CH <sub>2</sub> Cl <sub>2</sub> , 298 K, $\epsilon_S = 8.93$ ) .....	11
<b>Table S6:</b> Time constants for the different excited processes as observed from the fsTA measurements of <b>SC-SPDI<sub>2</sub></b> and <b>SC-NPDI<sub>2</sub></b> in different solvents .....	11

<b>Table S7:</b> Energy ( $\Delta E$ ), oscillator strength ( $f$ ), mean position ( $POR$ ), participation ratio ( $PR$ ) of initial orbital (hole) and final orbital (electron) and charge transfer character ( $CT$ ) of singlet states in <b>SC-SPDI<sub>2</sub></b> in the FC geometry.....	12
<b>Table S8:</b> Energy ( $\Delta E$ ), oscillator strength ( $f$ ), mean position ( $POR$ ), participation ratio ( $PR$ ) of initial orbital (hole) and final orbital (electron) and charge transfer character ( $CT$ ) of singlet states in <b>SC-NPDI<sub>2</sub></b> in the FC geometry.....	12
<b>Table S9:</b> Energy ( $\Delta E$ ), oscillator strength ( $f$ ), mean position ( $POR$ ), participation ratio ( $PR$ ) of initial orbital (hole) and final orbital (electron) and charge transfer character ( $CT$ ) of singlet states in <b>SC-SPDI<sub>2</sub></b> in the relaxed foldamer geometry. ....	12
<b>Table S10:</b> Energy ( $\Delta E$ ), oscillator strength ( $f$ ), mean position ( $POR$ ), participation ratio ( $PR$ ) of initial orbital (hole) and final orbital (electron) and charge transfer character ( $CT$ ) of singlet states in <b>SC-NPDI<sub>2</sub></b> in the relaxed foldamer geometry. ....	12
<b>Section 4: Figures</b> .....	<b>13</b>
<b>Figure S1:</b> Optimised structures of core annulated perylenediimide monomers a) <b>SPDI</b> and b) <b>NPDI</b> showing the in-plane bend in the perylene core.....	13
<b>Figure S2:</b> Optimised structures of core annulated perylenediimide monomers a) <b>SPDI</b> and b) <b>NPDI</b> showing the C-S and C-N bond lengths.....	13
<b>Figure S3:</b> Normalised absorption spectra of sulphur annulated ( <b>SPDI</b> ) and nitrogen annulated ( <b>NPDI</b> ) perylenediimide monomers compared to unsubstituted <b>PDI</b> .....	13
<b>Figure S4:</b> Optimized geometries of the dimers a) <b>SC-SPDI<sub>2</sub></b> and b) <b>SC-NPDI<sub>2</sub></b> in the excited state showing the $\pi$ -stacked foldamer-like geometry viewed from two different axis. The centroid to centroid distance ( $d$ ) and the torsional/dihedral angles ( $\varphi$ ) between the chromophores are also indicated in the figure. ....	14
<b>Figure S5:</b> Molecular structure of <b>di-PDI</b> . ....	14
<b>Figure S6:</b> Potential energy curve of the dimers a) <b>SC-NPDI<sub>2</sub></b> and b) <b>SC-SPDI<sub>2</sub></b> in the ground state with varying torsional angles. ....	14
<b>Figure S7:</b> a)Time-resolved emission spectra (TRES, $\lambda_{ex} = 478$ nm) of <b>SC-SPDI<sub>2</sub></b> in TOL, b) Evolution associated spectra (EAS), (c) the relative population profiles of <b>SC-SPDI<sub>2</sub></b> in TOL and d) normalized evolution associated spectra. The orange (A, EAS <sub>A</sub> ) and green (B, EAS <sub>B</sub> ) colored spectrum and decay profiles correspond to emission from the unrelaxed (Ex*) and relaxed (Ex) excimer states. ....	15
<b>Figure S8:</b> a)Time-resolved emission spectra (TRES, $\lambda_{ex} = 478$ nm) of <b>SC-NPDI<sub>2</sub></b> in TOL, b) ) Evolution associated spectra (EAS), (c) the relative population profiles of <b>SC-NPDI<sub>2</sub></b> in TOL and d) normalized evolution associated spectra. The orange (A, EAS <sub>A</sub> ) and green (B, EAS <sub>B</sub> ) colored spectrum and decay profiles corresponds to emission from the unrelaxed (Ex*) and relaxed (Ex) excimer states. ....	15
<b>Figure S9:</b> Comparison between the steady-state emission spectra (top) with the time-resolved emission spectra (bottom) of a) <b>SC-SPDI<sub>2</sub></b> and b) <b>SC-NPDI<sub>2</sub></b> recorded in TOL. The highlighted region in the spectra represents the emission maximum. ....	16
<b>Figure S10:</b> Steady-state UV-vis absorption spectra along with emission spectra (recorded at 90K and 297K) of a) <b>SC-SPDI<sub>2</sub></b> and b) <b>SC-NPDI<sub>2</sub></b> in TOL.....	16
<b>Figure S11:</b> a) Emission spectra of <b>SPDI</b> at room temperature and <b>SC-SPDI<sub>2</sub></b> at 90K and b) Emission spectra of <b>NPDI</b> at room temperature and <b>SC-NPDI<sub>2</sub></b> at 90K in TOL. ....	16
<b>Figure S12:</b> Comparison of time-resolved emission spectra with steady-state emission spectra at different temperatures for a) <b>SC-SPDI<sub>2</sub></b> and b) <b>SC-NPDI<sub>2</sub></b> in TOL. ....	17
<b>Figure S13:</b> a) Absorption spectra and excitation spectra of <b>SC-SPDI<sub>2</sub></b> in toluene and polystyrene matrix respectively, b) Emission spectra of <b>SC-SPDI<sub>2</sub></b> in polystyrene matrix and toluene, c) Absorption spectra and excitation spectra of <b>SC-NPDI<sub>2</sub></b> in toluene and polystyrene matrix respectively, d) Emission spectra of <b>SC-NPDI<sub>2</sub></b> in polystyrene matrix and toluene .....	17

<b>Figure S14:</b> Solvent-dependent absorption and emission spectra of a) <b>SC-NPDI<sub>2</sub></b> and b) <b>SC-SPDI<sub>2</sub></b> .....	18
<b>Figure S15:</b> Normalised absorption and emission spectra of (a, b) <b>SPDI</b> and (c, d) <b>NPDI</b> in different solvents. .....	18
<b>Figure S16:</b> Normalised excitation spectra of a) <b>SPDI</b> , b) <b>NPDI</b> , c) <b>SC-SPDI<sub>2</sub></b> and d) <b>SC-NPDI<sub>2</sub></b> collected at emission maximum in different solvents. ....	19
<b>Figure S17:</b> Solvent-dependent normalized emission spectra of a) <b>SC-SPDI<sub>2</sub></b> and b) <b>SC-NPDI<sub>2</sub></b> .....	19
<b>Figure S18:</b> Fluorescence decay profiles of a) <b>SC-SPDI<sub>2</sub></b> and b) <b>SC-NPDI<sub>2</sub></b> in different solvents. The fluorescence decay profile of <b>SC-NPDI<sub>2</sub></b> in ACN is biexponentially fitted. The second component is assigned to scattering contribution as <b>SC-NPDI<sub>2</sub></b> has very low fluorescence quantum yield in ACN (<0.1%).....	20
<b>Figure S19:</b> Fluorescence decay profiles of (a) <b>SPDI</b> and (b) <b>NPDI</b> in different solvents. ....	20
<b>Figure S20:</b> (a, c) Cyclic voltammetry data and (b, d) differential pulse voltammograms of <b>SC-SPDI<sub>2</sub></b> and <b>SC-NPDI<sub>2</sub></b> in CH <sub>2</sub> Cl <sub>2</sub> . (Tetrabutylammonium hexafluorophosphate (0.1 M) as the supporting electrolyte, scan rate 100 mV s <sup>-1</sup> . Fc/Fc+=ferrocene/ferrocenium couple).....	21
<b>Figure S21:</b> Energy level diagram with the frontier molecular orbitals of <b>SPDI</b> and <b>SC-SPDI<sub>2</sub></b> . ....	21
<b>Figure S22:</b> Energy level diagram with the frontier molecular orbitals of <b>NPDI</b> and <b>SC-NPDI<sub>2</sub></b> .....	22
<b>Figure S23:</b> Femtosecond transient absorption spectra (top), evolution associated spectra (EAS, middle) and population profiles (bottom) of <b>SPDI</b> in different solvents. ....	22
<b>Figure S24:</b> Femtosecond transient absorption spectra (top), evolution associated spectra (EAS, middle) and population profiles (bottom) of <b>NPDI</b> in different solvents. ....	23
<b>Figure S25:</b> Global analysis fits for selected fsTA wavelengths of <b>SC-SPDI<sub>2</sub></b> ( $\lambda_{ex} = 470$ nm) in toluene to A→B→C→D kinetic model. Fits are shown as solid lines. Evolution associated spectra (EAS, b) and population profiles (c) of <b>SC-SPDI<sub>2</sub></b> in toluene. ....	23
<b>Figure S26:</b> Femtosecond transient absorption spectra (top), Evolution associated spectra (bottom) of <b>SC-NPDI<sub>2</sub></b> in toluene. ....	24
<b>Figure S27:</b> Global analysis fits for selected fsTA wavelengths of <b>SC-NPDI<sub>2</sub></b> ( $\lambda_{ex} = 470$ nm) in toluene to A→B→C→D kinetic model. Fits are shown as solid lines. Evolution associated spectra (EAS, b) and population profiles (c) of <b>SC-NPDI<sub>2</sub></b> in toluene. ....	24
<b>Figure S28:</b> Comparison between the steady-state emission spectra (top) with the evolution associated spectra (bottom) of a) <b>SC-SPDI<sub>2</sub></b> and b) <b>SC-NPDI<sub>2</sub></b> recorded in TOL.....	25
<b>Figure S29:</b> Femtosecond transient absorption spectra, Evolution associated spectra (EAS, bottom) of <b>SC-SPDI<sub>2</sub></b> in acetone. ....	25
<b>Figure S30:</b> Global analysis fits for selected fsTA wavelengths of <b>SC-SPDI<sub>2</sub></b> ( $\lambda_{ex} = 470$ nm) in acetone to A→B→C→D kinetic model. Fits are shown as solid lines. Evolution associated spectra (EAS, b) and population profiles (c) of <b>SC-SPDI<sub>2</sub></b> in acetone. ....	26
<b>Figure S31:</b> Global analysis fits for selected fsTA wavelengths of <b>SC-SPDI<sub>2</sub></b> ( $\lambda_{ex} = 470$ nm) in acetonitrile to A→B→C→D kinetic model. Fits are shown as solid lines. Evolution associated spectra (EAS, b) and population profiles (c) of <b>SC-SPDI<sub>2</sub></b> in acetonitrile.....	26
<b>Figure S32:</b> UV-vis absorption changes of <b>SPDI</b> in ACN upon the addition of a) antimony pentachloride (SbCl <sub>5</sub> ) and b) cobaltocene (CoCp <sub>2</sub> ). ....	27
<b>Figure S33:</b> UV-Vis absorption spectra for the electrochemical reduction of a) <b>SPDI</b> and b) <b>NPDI</b> . ....	27
<b>Figure S34:</b> UV-vis absorption changes of <b>NPDI</b> in ACN upon the addition of a) antimony pentachloride (SbCl <sub>5</sub> ) and b) cobaltocene (CoCp <sub>2</sub> ). ....	27
<b>Figure S35:</b> Femtosecond transient absorption spectra (top), Evolution associated spectra (EAS, bottom) of <b>SC-NPDI<sub>2</sub></b> in a) acetone and b) acetonitrile. ....	28

<b>Figure S36:</b> Global analysis fits for selected fsTA wavelengths of <b>SC-SPDI<sub>2</sub></b> ( $\lambda_{\text{ex}} = 470 \text{ nm}$ ) in acetone to A→B→C→D kinetic model. Fits are shown as solid lines. Evolution associated spectra (EAS, b) and population profiles (c) of <b>SC-NPDI<sub>2</sub></b> in acetone. ....	28
<b>Figure S37:</b> Global analysis fits for selected fsTA wavelengths of <b>SC-SPDI<sub>2</sub></b> ( $\lambda_{\text{ex}} = 470 \text{ nm}$ ) in acetone to A→B→C→D kinetic model. Fits are shown as solid lines. Evolution associated spectra (EAS, b) and population profiles (c) of <b>SC-NPDI<sub>2</sub></b> in acetonitrile. ....	29
<b>Figure S38:</b> fsTA spectra highlighting the change in intensities of 0-0 and 0-1 vibronic bands for <b>SC-SPDI<sub>2</sub></b> and <b>SC-NPDI<sub>2</sub></b> in different solvents. ....	29
<b>Figure S39:</b> (Top) Nanosecond transient absorption spectra of <b>SC-SPDI<sub>2</sub></b> in (a) TOL, (b) ACE and (c) ACN showing the excited-state dynamics after photoexcitation in N <sub>2</sub> atmosphere. (Bottom) Evolution associated spectra were reconstructed from global analysis of the A → GS model in all solvents. ....	30
<b>Figure S40:</b> (Top) Nanosecond transient absorption spectra of <b>SC-NPDI<sub>2</sub></b> in (a) TOL, (b) ACE and (c) ACN showing the excited-state dynamics after photoexcitation in N <sub>2</sub> atmosphere. (Bottom) Evolution associated spectra were reconstructed from global analysis of the A → GS model in all solvents. ....	30
<b>Figure S41:</b> Nanosecond transient absorption spectra of <b>SC-SPDI<sub>2</sub></b> in a) ACN, b) ACE, c) TOL and of <b>SC-NPDI<sub>2</sub></b> in d) ACN, e) ACE, f) TOL after O <sub>2</sub> purging. ....	31
<b>Figure S42:</b> Comparison between the EAS from fsTA measurements (top) and nTA spectra (bottom) for a) <b>SC-NPDI<sub>2</sub></b> and b) <b>SC-SPDI<sub>2</sub></b> . ....	31
<b>Figure S43:</b> Schematic potential energy surface of <b>SC-SPDI<sub>2</sub></b> in TOL summarising the excited state dynamics. ....	32
<b>Figure S44:</b> Schematic potential energy surface of <b>SC-SPDI<sub>2</sub></b> in ACE and ACN summarising the excited state dynamics. ....	32
<b>Figure S45:</b> Schematic potential energy surface of <b>SC-NPDI<sub>2</sub></b> in TOL summarising the excited state dynamics. ....	33
<b>Figure S46:</b> Schematic potential energy surface of <b>SC-NPDI<sub>2</sub></b> in ACE and ACN summarising the excited state dynamics. ....	33
<b>Figure S47:</b> Molecular structures of the dimers and the corresponding PR and CT values for the transition to the first singlet excited state along with the electron-hole correlation plots (a,b) <b>SC-SPDI<sub>2</sub></b> and (c,d) <b>SC-NPDI<sub>2</sub></b> . ....	34
<b>Figure S48:</b> Hole and electron isosurfaces for the first six singlet excited state transitions and the corresponding electron-hole correlation plots of <b>SC-NPDI<sub>2</sub></b> in the near-orthogonal geometry. ....	34
<b>Figure S49:</b> Hole and electron isosurfaces for the first six singlet excited state transitions along with the corresponding electron-hole correlation plots of <b>SC-SPDI<sub>2</sub></b> in the near-orthogonal geometry. ....	35
<b>Figure S50:</b> Hole and electron isosurfaces for the first six singlet excited state transitions along with the corresponding electron-hole correlation plots of <b>SC-NPDI<sub>2</sub></b> in the foldamer geometry. ....	35
<b>Figure S51:</b> Hole and electron isosurfaces for the first six singlet excited state transitions along with the corresponding electron-hole correlation plots of <b>SC-SPDI<sub>2</sub></b> in the foldamer geometry. ....	36

## Section 1: Materials and Methods

All chemicals were obtained from commercial suppliers and used as received without further purification. All reactions were carried out in oven-dried glassware prior to use. Solvents were dried and distilled by standard laboratory purification techniques. TLC analyses were performed on recoated aluminum plates of silica gel 60 F254 plates (0.25 mm, Merck), and developed TLC plates were visualized under short and long-wavelength UV lamps. Flash column chromatography was performed using silica gel of 200-400 mesh employing a solvent polarity correlated with the TLC mobility observed for the substance of interest. Yields refer to chromatographically and spectroscopically homogenous substances.  $^1\text{H}$  and  $^{13}\text{C}$  NMR spectra were measured on a 500 MHz Bruker avance DPX spectrometer. The internal standard used for  $^1\text{H}$  and  $^{13}\text{C}$  NMR is tetramethylsilane (TMS). High-resolution mass spectra (HRMS) were recorded on Thermo scientific Q exactive mass spectrometer using the Atmospheric pressure chemical ionization (APCI, positive mode) technique. Photophysical measurements of the derivatives were carried out in a cuvette of 3 mm path length. Absorption and emission spectra were recorded on Shimadzu UV-3600 UV-VIS-NIR and Horiba Jobin Yvon Fluorolog spectrometers, respectively. Lifetime measurements were carried out in an IBH picosecond time-correlated single-photon counting (TCSPC) system. The pulse width of the excitation ( $\lambda_{\text{exci}} = 478 \text{ nm}$ ) source is determined to be  $<100 \text{ ps}$ , and 495 nm long-pass filter (Newport) was used to minimize the scatter arising from the laser source. The fluorescence decay profiles were de-convoluted using DAS6.3 and fitted with exponential decay, minimizing the  $\chi^2$  values. Temperature-dependent (90K-250K) photoluminescence measurements were carried out using liquid nitrogen cryostat (Janis VNF-100). Dilute thin films (1% in polystyrene) of dimers (**SC-SPDI**<sub>2</sub> and **SC-NPDI**<sub>2</sub>) were prepared from toluene solution on quartz to examine the effect of rigidification on excited-state decay dynamics.

### 1.1 Computational Analysis

All the calculations are carried out in Gaussian 16 employing the b3lyp functional with Grimme's d3 dispersion and def2svp basis set at the DFT level of theory unless stated otherwise.<sup>1</sup> Vertical excitation energies and oscillator strengths were calculated employing time-dependent DFT (TD-DFT) at the  $\omega\text{b97xd/def2svp}$  level of theory. The frontier molecular orbitals (FMO) of monomers and dimers were obtained from the generated cube files of energy calculations. Hole-electron analyses were carried out using Multiwfn version 3.7.8.<sup>2</sup> Multiwfn uses post-processed Gaussian 16 output files generated at  $\omega\text{b97xd/def2svp}$  level of theory for the respective analyses. 3-pentane and hexane alkane chains in the dimers and monomers were replaced with methane group during the computation calculation in order to reduce the computational cost.

### 1.2 Time-Resolved Emission Spectra (TRES) Analysis

Time-resolved emission spectral (TRES) measurements followed by global analysis (GA) of the kinetic traces (at all wavelengths) were performed in an IBH picosecond time-correlated single-photon counting (TCSPC) system and glotaran<sup>3</sup> software, respectively. The singular value decomposition (SVD) followed by the GA of the time vs. wavelength plots furnished a evolution associated spectra (EAS) based deconvolution of the temporal components in the fluorescence emission. Time-resolved emission spectral (TRES) investigation of **SC-SPDI**<sub>2</sub> and **SC-NPDI**<sub>2</sub> in toluene was carried out by exciting at 478 nm (DD-470L; DD-470L; pulse width  $<60 \text{ ps}$ ).

### 1.3 Electrochemistry

Cyclic voltammograms and differential pulse voltammograms were acquired on CH instruments, inc electrochemical workstation at room temperature, employing a three-electrode single-compartment cell: glassy carbon electrode as the working electrode, a Pt wire as the counter electrode, and silver wire as the reference electrode. Working and reference electrodes were polished on a felt pad with  $0.05 \mu\text{m Al}_2\text{O}_3$  suspension, sonicated in acetone for about 3 minutes, and dried before each experiment; the Pt wire was flame-cleaned. The supporting electrolyte, tetrabutylammonium hexafluorophosphate (TBAF), was previously dried under vacuum, dichloromethane was degassed prior to use, and all measurements were performed under a nitrogen atmosphere. The concentration of TBAF used was typically 100 times of the

analyte. Calibration of the instrument was performed using the ferrocene/ferrocenium (Fc/Fc<sup>+</sup>) redox couple as an external standard and measured under the same condition before and after the measurement of samples.  $E_{Fc/Fc^+}$  is the potential of Fc/Fc<sup>+</sup> vs. Ag. The energy level of Fc/Fc<sup>+</sup> was assumed to be -4.8 eV with respect to vacuum.<sup>4</sup> HOMO and LUMO energies were calculated using the following equation.<sup>5</sup>

$$E_g^{opt} = 1240/\lambda_{onset} \quad S1$$

$$E_{LUMO} = -(E'_{red} + 4.8 - E_{Fc/Fc^+}) \text{ eV} \quad S2$$

$$E_{HOMO} = E_{LUMO} - E_g^{opt} \quad S3$$

respectively, where  $E'_{red}$  are the experimentally measured reduction potentials vs. Ag.  $E_{LUMO}$  and  $E_{HOMO}$  are the corresponding to LUMO and HOMO energy levels.

#### 1.4 Weller Analysis

The change in free energy for the charge-separation and charge recombination ( $\Delta G$ ) were estimated employing the followed relations based on the Born dielectric continuum model.<sup>6</sup>

$$\Delta G_{CS} = e[E_{ox} - E_{red}] - E_{00} + C + S \quad S4$$

$$C = \frac{-e^2}{4\pi\epsilon_0} \left( \frac{1}{\epsilon_S r_{AD}} \right) \quad S5$$

$$S = \frac{e^2}{8\pi\epsilon_0} \left( \frac{1}{r_D} + \frac{1}{r_A} \right) \left( \frac{1}{\epsilon_S} - \frac{1}{\epsilon_{SP}} \right) \quad S6$$

$$\Delta G_{CR} = -(E_{00} + \Delta G_{CS}) \quad S7$$

Where  $e$  is the charge of the electron,  $E_{ox}$  and  $E_{red}$  are the oxidation and reduction potentials, respectively,  $\epsilon_0$  is the permittivity of free space,  $\epsilon_S$  is the static dielectric constant of the solvent, and  $\epsilon_{SP}$  is the static dielectric constant of the solvent used for electrochemical measurements,  $r_{AD}$  is the donor-acceptor distance,  $r_D$  and  $r_A$  are the cation and anion hard-sphere radii, respectively ( were approximated as  $\frac{r_{AD}}{2}$ ) and  $E_{00}$  is the energy of the excited singlet (donor) state. At finite distances, the Coulombic attraction energy between(C) the radical ion-is given by a point-charge model as  $\left( \frac{1}{\epsilon_S r_{AD}} \right)$ . Since SC-SPDI<sub>2</sub> and SC-NPDI<sub>2</sub> exhibit excimer formation in all the solvents, the optical bandgap ( $E_{00}$ , the precursor of SB-CS) was determined by the intersection of the normalized absorption and emission spectra of monomeric **SPDI** and **NPDI**.

#### 1.5 Femtosecond transient absorption (fsTA) measurement

A Spectra-Physics Mai Tai SP mode-locked laser (86 MHz, 800 nm) was used as a seed for a Spectra-Physics Spitfire ace regenerative amplifier (1 kHz, 5.5 mJ). A fraction of the amplified output was used to produce a 470 nm pump pulse by TOPAS. A residual pulse of 800 nm was sent through an optical delay line inside an ExciPro pump-probe spectrometer to produce a white light continuum by employing a sapphire crystal. The white light continuum was split into two, and the streams were used as a probe and reference pulses. The femtosecond transient absorption spectra of the sample were recorded using a dual diode array detector, having a 200 nm detection window and 3.5 ns optical delay. Sample solutions were prepared in a rotating cuvette with a 1.2 mm path length. Determination of an appropriate instrument response function (IRF) is needed for accurate deconvolution of recorded transient absorption data. The IRF was determined by a solvent (10% benzene in methanol) two-photon absorption and was found to be ~110 fs at about 530 nm. A neutral density filter (80%) was used for controlling the incident flux on the sample. fsTA measurement of dimers and monomers in different solvents were recorded by photoexciting the sample with 470 nm, 200 nJ, and 100 fs pulses to moderate singlet-singlet annihilation that often arises in multi-chromophoric assemblies.<sup>7</sup> The observed kinetic components were laser intensity-independent, ruling out the chance of singlet-singlet annihilation.

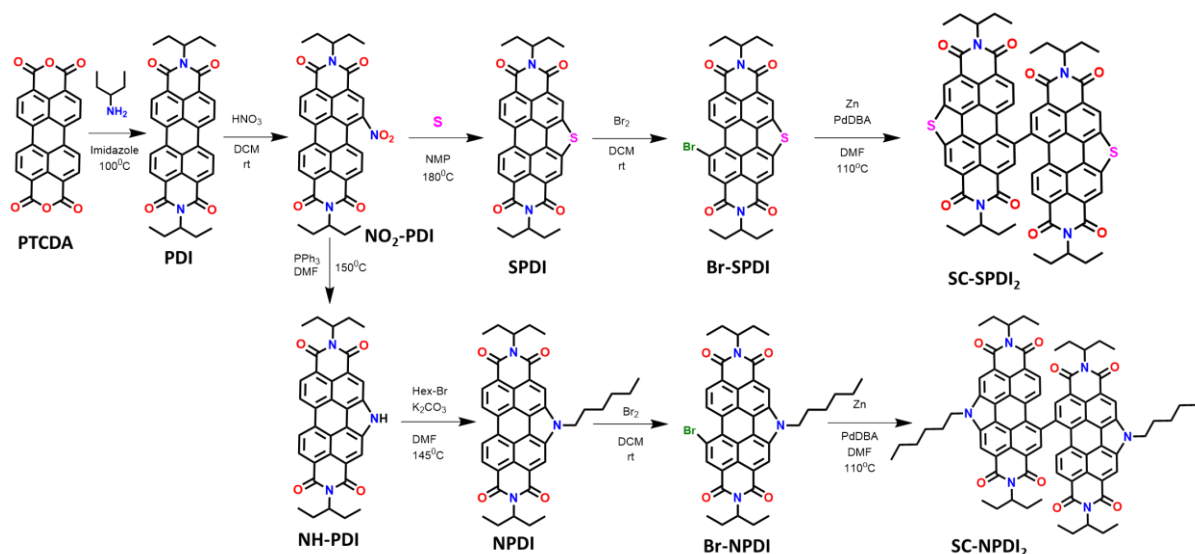
## 1.6 Global Analysis

Target analyses of the fsTA spectra were performed using the Glotaran software.<sup>3</sup> The procedure evaluates the instrument time response function and the group velocity dispersion of the white continuum and allows one to compute decay time constants and dispersion-compensated spectra. All the wavelengths were analyzed in target analysis concurrently, employing a target model to give evolution associated spectra (EAS). The EAS indicates that the evolution of the spectra in time does not necessarily denote a real physical/chemical species. EAS designates the spectral changes that occur with their associated time constants.

## 1.7 TheoDORE Analysis

The excitations of orthogonally arranged core annulated perylenediimide dimers at the DFT optimized structure were analyzed using TheoDORE.<sup>8,9</sup> The calculations were carried out in Gaussian 16 at TD- $\omega$ b97xd/def2svp level of theory. For the dimer systems under investigation, each monomer is considered as a fragment. The parameters used to investigate the excited state characteristics are participation ratio (PR), mean position (POS) of initial orbital (hole) and final orbital (electron), and charge transfer character (CT). The magnitude of PR relates to the number of fragments participating in the excitation; hence, and ranges from 1 to 2. When the exciton localized one fragment, PR $\approx$ 1.0 and PR $\approx$ 2.0 when the exciton delocalized in both fragments. POS provides the mean position of hole and electron for a particular excitation. Charge transfer states and delocalized Frenkel states show POS = 1.5. If the Frenkel state is localized on monomer A, then POS = 1, and if localized on monomer B, POS = 2, for a dimer AB. Finally, CT is related to the total weight of configurations where initial and final orbitals are situated on different fragments. A CT value of 1 denotes the presence of a charge-separated state, and CT = 0 refers to Frenkel states. Further, electron-hole correlation plots were generated for analyzing the excitonic character for the perylenediimide dimer systems. If the shade is present only in the off-diagonal parts, the excitonic character is Frenkel. Diagonal shades refer to a CT state.

## Section 2: Synthesis and Characterization



**Scheme S1:** Showing the synthesis scheme for monomers (**SPDI** and **NPDI**) and dimers (**SC-SPDI<sub>2</sub>** and **SC-NPDI<sub>2</sub>**).

### Synthesis of NPDI:

The synthesis of **NPDI** was carried out following reported procedures.<sup>10</sup> **NH-PDI**, 0.50 g, 0.92 mmol) and potassium carbonate (0.25 g, 1.8 mmol) were added to a round-bottom flask. Approximately 20 mL Dry N,N'-dimethylformamide was added, followed by the addition of 1-bromo-hexane (0.27 g, 1.7 mmol). The reaction mixture was purged with nitrogen followed by heating at 170 °C for 1 hour. After the completion of the reaction, the reaction mixture was cooled to room temperature. The compound was extracted using water and dichloromethane. The organic phase was collected and the solvent was removed using a rotary evaporator to give a crude solid. The crude product was purified using column chromatography. The product fraction was collected and the solvent was removed in vacuo to give a red solid. **Yield:** 65%

**NPDI: 1H NMR** (500 MHz, CDCl<sub>3</sub>, ppm)  $\delta$  = 8.91 (s, 2H), 8.87-8.84 (m, 2H), 8.82-8.76 (m, 2H), 5.30-5.21 (m, 2H), 4.80 (t, 2H), 2.46-2.34 (m, 4H), 2.20-2.12 (m, 2H), 2.11-2.01 (m, 4H), 1.45-1.28 (m, 6H), 1.03 (t, 12H), 0.87 (t, 3H)

**13C NMR** (500 MHz, CDCl<sub>3</sub>, ppm)  $\delta$  = 133.71, 131.57, 123.59, 122.76, 120.72, 118.42, 56.77, 45.91, 30.47, 30.30, 25.81, 24.22, 21.42, 12.90, 10.47

**HRMS** (APCI) *m/z* calculated for C<sub>40</sub>H<sub>42</sub>N<sub>3</sub>O<sub>4</sub>[(M+H)<sup>+</sup>]: 628.3175, Observed: 628.3164

### Synthesis of SPDI:

The synthesis of **SPDI** was carried out following modified reported procedures.<sup>11</sup> Sulfur (160 mg, 4.9 mmol) was dissolved in N-methylpyrrolidone (12 mL, 70°C). Compound **NO<sub>2</sub>-PDI** (0.50 g, 0.62 mmol) was added under nitrogen to the round-bottom flask. The mixture was heated (130°C, ca. 75 min, until the starting material could not be detected by TLC). After the completion of the reaction, the reaction mixture was poured into water (150 mL) and the precipitate was collected by vacuum filtration followed by washing with water. The mixture is dried and purified by column chromatography. **Yield:** 52%

**SPDI: 1H NMR** (500 MHz, CDCl<sub>3</sub>, ppm)  $\delta$  = 9.204 (d, 2H), 8.826 (d, 4H), 5.144 (m, 2H), 2.286-2.53 (m, 4H), 1.96-1.932 (m, 4H), 0.915 (t, 12H)

**13C NMR** (500 MHz, CDCl<sub>3</sub>, ppm)  $\delta$  = 137.20, 132.18, 130.46, 125.26, 122.54, 122.16, 76.25, 75.99, 56.97, 24.11, 10.41

**HRMS** (APCI) *m/z* calculated for C<sub>34</sub>H<sub>29</sub>N<sub>2</sub>O<sub>4</sub>S[(M+H)<sup>+</sup>]: 561.1848, Observed: 561.1842

### Synthesis of SC-NPDI<sub>2</sub>:

The synthesis of **SC-NPDI<sub>2</sub>** was carried out following the reported procedures.<sup>10</sup> **Br-NPDI** (0.37 g, 0.52 mmol) and zinc dust (170 mg, 2.6 mmol) were added to a 20 mL roundbottom flask. Approximately 40 mg of bis(dibenzylideneacetone)palladium (0) was added to the mixture. The flask was sealed under a nitrogen atmosphere and 20 mL of N,N-dimethylformamide was added. The reaction mixture was purged with nitrogen for 10 minutes and was heated to ~100 °C for 2.5 hours. After the completion of the reaction, the crude solid obtained after removing the solvent in vacuo was purified using column chromatography. A dark red solid was obtained after the initial purification. For further purification, the red solid was boiled in 100 mL of isopropanol with vigorous stirring for approximately 1 hour followed by cooling to room temperature and filtration using a Buchner funnel, resulting in a bright red solid. **Yield:** 38%.

**SC-NPDI<sub>2</sub>: 1H NMR** (500 MHz, CDCl<sub>3</sub>, ppm)  $\delta$  = 9.30 (s, 2H), 9.12 (s, 2H), 8.91 (s, 2H), 7.99 (s, 2H), 7.74-7.72 (m, 2H), 5.35-5.16 (m, 4H), 5.07-5.04 (m, 4H), 2.42-2.31 (m, 8H), 2.28-2.16 (m, 4H), 2.07-2.00 (m, 4H), 1.93-1.84 (m, 4H), 1.64-1.56 (m, 4H), 1.50-1.45 (m, 4H), 1.42-1.37 (m, 4H), 1.06-0.82 (m, 30H).

**13C NMR** (500 MHz, CDCl<sub>3</sub>, ppm)  $\delta$  = 139.87, 134.25, 134.03, 131.89, 129.37, 125.81, 123.94, 123.69, 122.55, 121.73, 119.08, 118.81, 56.98, 56.59, 46.12, 30.66, 30.43, 25.99, 24.02, 21.52, 13.00, 10.49, 10.22  
**HRMS** (APCI) m/z calculated for C<sub>80</sub>H<sub>81</sub>N<sub>6</sub>O<sub>8</sub>[(M+H)<sup>+</sup>]: 1253.6115, Observed: 1253.6112

### Synthesis of SC-SPDI<sub>2</sub>:

The synthesis of **SC-SPDI<sub>2</sub>** was carried out following the modified procedures (Scheme 1).<sup>11</sup> **Br-SPDI** (0.33 g, 0.52 mmol) and zinc dust (170 mg, 2.6 mmol) were added to a 20 mL roundbottom flask. Approximately 40 mg of bis(dibenzylideneacetone)palladium(0) was added to the mixture. The flask was sealed under a nitrogen atmosphere and 20 mL of N,N-dimethylformamide was added. The reaction mixture was purged with nitrogen for 10 minutes and was heated to ~100 °C for 2.5 hours. After the completion of the reaction, the crude solid obtained after removing the solvent in vacuo was purified using column chromatography. A dark red solid was obtained after the initial purification. For further purification, the red solid was boiled in 100 mL of isopropanol with vigorous stirring for approximately 1 hour followed by cooling to room temperature and filtration using a Buchner funnel, resulting in a bright red solid. **Yield:** 48%

**SC-SPDI<sub>2</sub>: 1H NMR** (500 MHz, CDCl<sub>3</sub>, ppm)  $\delta$  = 9.61 (s, 2H), 9.45 (s, 2H), 8.81 (s, 2H), 8.18-8.10 (m, 4H), 5.30-4.93 (m, 4H), 2.38-2.30 (m, 4H), 2.27-2.16 (m, 4H), 2.04-1.96 (m, 4H), 1.94-1.85 (m, 4H), 1.04-0.83 (m, 24H).

**13C NMR** (500 MHz, CDCl<sub>3</sub>, ppm)  $\delta$  = 140.81, 138.99, 138.42, 133.30, 131.95, 131.63, 130.86, 129.04, 128.23, 126.96, 126.52, 125.26, 124.19, 58.23, 57.87, 31.94, 29.71, 29.38, 24.98, 24.93, 22.71, 14.14, 11.47, 11.23.

**HRMS** (APCI) m/z calculated for C<sub>68</sub>H<sub>55</sub>N<sub>4</sub>O<sub>8</sub>S<sub>2</sub>[(M+H)<sup>+</sup>]: 1119.3461, Observed: 1119.3452

## Section 3: Tables

**Table S1:** Oscillator strength for different transitions of **SPDI** calculated at TD- $\omega$ B97XD/ def2svp level of theory.

Molecule	State	Oscillator Strength	Energy (eV)	Wavelength (nm)	Major Orbital Transition
SPDI	S <sub>1</sub>	0.7381	2.929	423.4	HOMO → LUMO
	S <sub>2</sub>	0.1113	3.432	361.3	HOMO-1 → LUMO
	S <sub>3</sub>	0.0023	4.010	309.2	HOMO-3 → LUMO
	S <sub>4</sub>	0.0004	4.106	302.0	HOMO-4 → LUMO
	S <sub>5</sub>	0	4.109	301.7	HOMO-5 → LUMO
	S <sub>6</sub>	0.0009	4.119	301.0	HOMO → LUMO+2 HOMO-2 → LUMO

**Table S2:** Oscillator strength for different transitions of **NPDI** calculated at TD- $\omega$ B97XD/ def2svp level of theory.

Molecule	State	Oscillator Strength	Energy (eV)	Wavelength (nm)	Major Orbital Transition
NPDI	S <sub>1</sub>	0.7381	2.872	431.7	HOMO → LUMO
	S <sub>2</sub>	0.1138	3.282	377.8	HOMO-1 → LUMO
	S <sub>3</sub>	0.0091	4.009	309.3	HOMO-2 → LUMO
	S <sub>4</sub>	0.0003	4.126	300.5	HOMO-4 → LUMO
	S <sub>5</sub>	0	4.132	300.0	HOMO-5 → LUMO
	S <sub>6</sub>	0.0001	4.139	299.6	HOMO-3 → LUMO HOMO → LUMO+2

**Table S3:** Oscillator strength for different transitions of **SC-SPDI<sub>2</sub>** calculated at TD- $\omega$ B97XD/ def2svp level of theory.

Molecule	State	Oscillator Strength	Energy (eV)	Wavelength (nm)	Major Orbital Transition
SC-SPDI <sub>2</sub>	S <sub>1</sub>	0.6818	2.906	426.6	HOMO → LUMO HOMO-1 → LUMO+1
	S <sub>2</sub>	0.6179	2.929	423.3	HOMO → LUMO+1 HOMO-1 → LUMO
	S <sub>3</sub>	0.3322	3.388	365.9	HOMO-2 → LUMO HOMO-3 → LUMO+1
	S <sub>4</sub>	0.0106	3.426	361.9	HOMO-3 → LUMO HOMO-2 → LUMO+1
	S <sub>5</sub>	0.0007	3.621	342.4	HOMO-1 → LUMO HOMO → LUMO+1
	S <sub>6</sub>	0.0050	3.622	342.3	HOMO → LUMO HOMO-1 → LUMO+1

**Table S4:** Oscillator strength for different transitions of **SC-NPDI<sub>2</sub>** calculated at TD- $\omega$ B97XD/ def2svp level of theory.

Molecule	State	Oscillator Strength	Energy (eV)	Wavelength (nm)	Major Orbital Transition
SC-NPDI <sub>2</sub>	S <sub>1</sub>	0.6211	2.826	438.7	HOMO → LUMO HOMO-1 → LUMO+1
	S <sub>2</sub>	0.6466	2.866	432.5	HOMO → LUMO+1 HOMO-1 → LUMO
	S <sub>3</sub>	0.3330	3.240	382.6	HOMO-2 → LUMO HOMO-3 → LUMO+1
	S <sub>4</sub>	0.0189	3.286	377.3	HOMO-3 → LUMO HOMO-2 → LUMO+1
	S <sub>5</sub>	0.0013	3.585	345.9	HOMO-1 → LUMO HOMO → LUMO+1
	S <sub>6</sub>	0.0170	3.595	344.9	HOMO → LUMO HOMO-1 → LUMO+1

**Table S5:** Summary of redox potentials and HOMO/LUMO calculations of **SC-SPDI<sub>2</sub>** and **SC-NPDI<sub>2</sub>** (CH<sub>2</sub>Cl<sub>2</sub>, 298 K,  $\epsilon_s = 8.93$ ).

Compound	<sup>b</sup> $E_{1(red)}$ (V)	<sup>b</sup> $E_{2(red)}$ (V)	<sup>b</sup> $E_{3(red)}$ (V)	<sup>b</sup> $E_{4(red)}$ (V)	$\lambda_{onset}$ (nm)	$E_g^{opt}$	HOMO (eV)	LUMO (eV)	$E_{00}$ (eV)
SC-SPDI <sub>2</sub>	-0.536	-0.616	-0.812	-0.920	527.00	2.35	-6.10	-3.74	-2.48
SC-NPDI <sub>2</sub>	-0.772	-0.820	-1.056	-1.184	551.95	2.25	-5.85	-3.60	-2.34

$E'_{red}$  is the reduction potential vs. Ag and  $E_{red}$  is the reduction potential vs. Fc/Fc<sup>+</sup>.

**Table S6:** Time constants for the different excited processes as observed from the fsTA measurements of **SC-SPDI<sub>2</sub>** and **SC-NPDI<sub>2</sub>** in different solvents.

		SC-NPDI <sub>2</sub>	SC-SPDI <sub>2</sub>
TOL	FE → Ex*	23.6 ± 0.2 ps	11.3 ± 0.1 ps
	Ex* → Ex	0.79 ± 0.02 ns	1.12 ± 0.02 ns
	Ex → Triplet/GS	7.87 ± 0.02 ns	8.10 ± 0.01 ns
ACE	FE → SB-CS	2.7 ± 0.02 ps	1.5 ± 0.1 ps
	SB-CS → Ex	1.66 ± 0.02 ns	2.01 ± 0.05 ns
	Ex → Triplet	3.82 ± 0.04 ns	5.89 ± 0.01 ns
ACN	FE → SB-CS	1.4 ± 0.01 ps	0.9 ± 0.1 ps
	SB-CS → Ex	0.71 ± 0.02 ns	0.84 ± 0.02 ns
	Ex → Triplet	2.30 ± 0.04 ns	5.81 ± 0.03 ns

FE: Frenkel exciton, Ex\*: Unrelaxed excimer, Ex: Relaxed excimer, SB-CS: Symmetry-Breaking Charge Separation

**Table S7:** Energy ( $\Delta E$ ), oscillator strength ( $f$ ), mean position ( $POR$ ), participation ratio ( $PR$ ) of initial orbital (hole) and final orbital (electron) and charge transfer character ( $CT$ ) of singlet states in **SC-SPDI**<sub>2</sub> in the FC geometry.

State	$\Delta E$ (eV)	$f$	POS	PR	CT
S <sub>1</sub>	2.906	0.682	1.5	2	0.026
S <sub>2</sub>	2.929	0.618	1.5	2	0.019
S <sub>3</sub>	3.388	0.332	1.5	2	0.023
S <sub>4</sub>	3.426	0.011	1.5	2	0.028
S <sub>5</sub>	3.621	0.001	1.5	2	0.937
S <sub>6</sub>	3.622	0.005	1.5	2	0.937

**Table S8:** Energy ( $\Delta E$ ), oscillator strength ( $f$ ), mean position ( $POR$ ), participation ratio ( $PR$ ) of initial orbital (hole) and final orbital (electron) and charge transfer character ( $CT$ ) of singlet states in **SC-NPDI**<sub>2</sub> in the FC geometry.

State	$\Delta E$ (eV)	$f$	POS	PR	CT
S <sub>1</sub>	2.826	0.621	1.498	2	0.038
S <sub>2</sub>	2.867	0.647	1.502	2	0.017
S <sub>3</sub>	3.24	0.333	1.5	2	0.021
S <sub>4</sub>	3.286	0.019	1.499	2	0.018
S <sub>5</sub>	3.585	0.001	1.501	1.971	0.947
S <sub>6</sub>	3.595	0.017	1.499	1.971	0.927

**Table S9:** Energy ( $\Delta E$ ), oscillator strength ( $f$ ), mean position ( $POR$ ), participation ratio ( $PR$ ) of initial orbital (hole) and final orbital (electron) and charge transfer character ( $CT$ ) of singlet states in **SC-SPDI**<sub>2</sub> in the relaxed foldamer geometry.

State	$\Delta E$ (eV)	$f$	POS	PR	CT
S <sub>1</sub>	2.094	0.082	1.5	2	0.375
S <sub>2</sub>	2.684	0.627	1.5	2	0.058
S <sub>3</sub>	2.788	0	1.5	2	0.873
S <sub>4</sub>	3.114	0.019	1.5	2	0.419
S <sub>5</sub>	3.145	0.405	1.5	2	0.27
S <sub>6</sub>	3.228	0.064	1.5	2	0.094

**Table S10:** Energy ( $\Delta E$ ), oscillator strength ( $f$ ), mean position ( $POR$ ), participation ratio ( $PR$ ) of initial orbital (hole) and final orbital (electron) and charge transfer character ( $CT$ ) of singlet states in **SC-NPDI**<sub>2</sub> in the relaxed foldamer geometry.

state	$\Delta E$ (eV)	$f$	POS	PR	CT
S <sub>1</sub>	1.938	0.063	1.5	2	0.394
S <sub>2</sub>	2.613	0.464	1.5	2	0.203
S <sub>3</sub>	2.756	0.141	1.5	2	0.731
S <sub>4</sub>	2.932	0.213	1.5	2	0.212
S <sub>5</sub>	3.149	0.216	1.5	2	0.483
S <sub>6</sub>	3.684	0.01	1.501	2	0.307

## Section 4: Figures

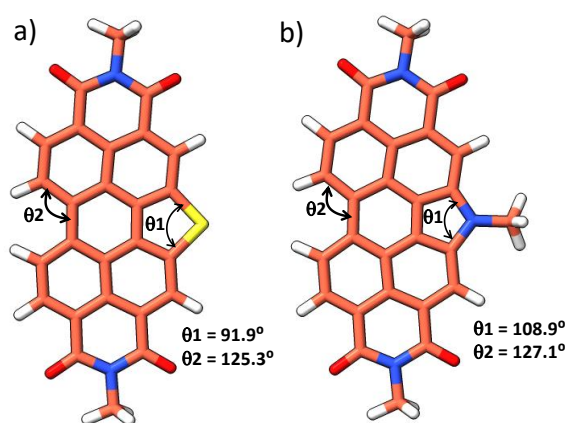


**Figure S1:** Optimised structures of core annulated perylene diimide monomers a) **SPDI** and b) **NPDI** showing the in-plane bend in the perylene core.

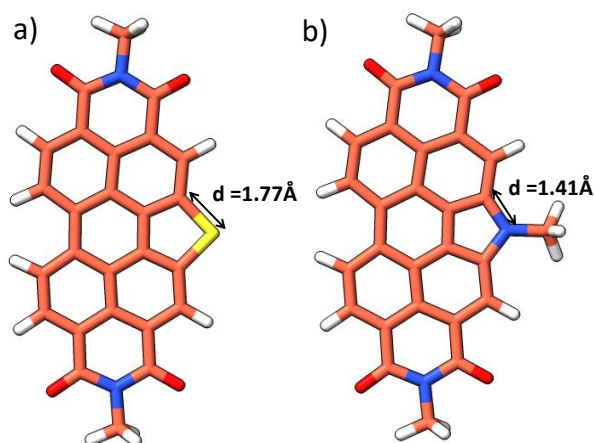


**Figure S2:** Optimised structures of core annulated perylene diimide monomers a) **SPDI** and b) **NPDI** showing the C-S and C-N bond lengths.

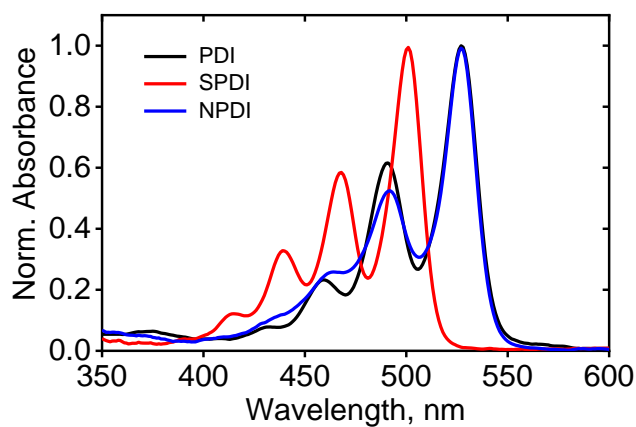


**Figure S3:** Normalised absorption spectra of sulphur annulated (**SPDI**) and nitrogen annulated (**NPDI**) perylene diimide monomers compared to unsubstituted **PDI**.

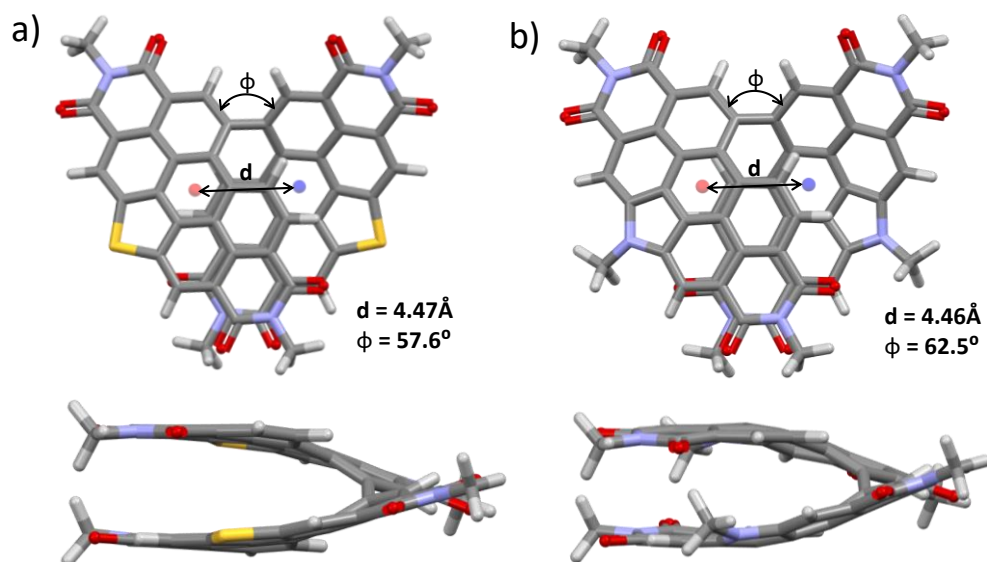


**Figure S4:** Optimized geometries of the dimers a) **SC-SPDI<sub>2</sub>** and b) **SC-NPDI<sub>2</sub>** in the excited state showing the  $\pi$ -stacked foldamer-like geometry viewed from two different axis. The centroid to centroid distance ( $d$ ) and the torsional/dihedral angles ( $\phi$ ) between the chromophores are also indicated in the figure.

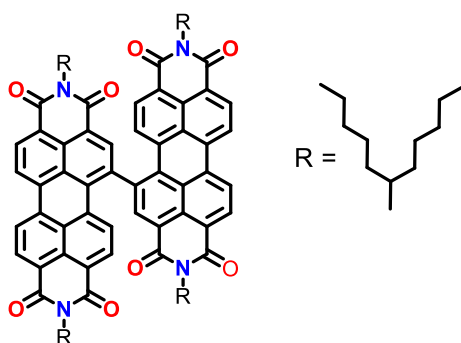


**Figure S5:** Molecular structure of **di-PDI**.

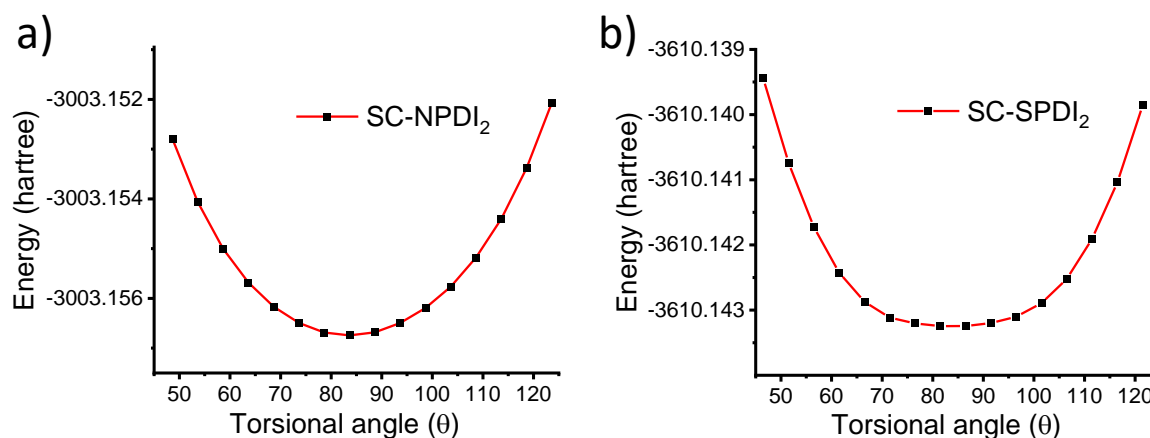


**Figure S6:** Potential energy curve of the dimers a) **SC-NPDI<sub>2</sub>** and b) **SC-SPDI<sub>2</sub>** in the ground state with varying torsional angles.

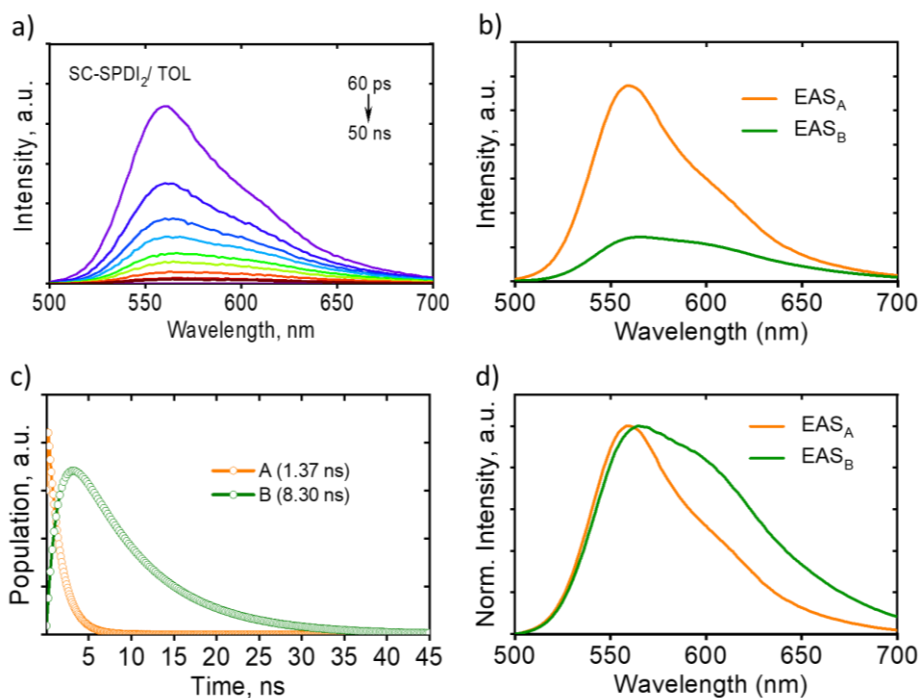


**Figure S7:** a) Time-resolved emission spectra (TRES,  $\lambda_{ex} = 478$  nm) of **SC-SPDI<sub>2</sub>** in TOL, b) Evolution associated spectra (EAS), (c) the relative population profiles of **SC-SPDI<sub>2</sub>** in TOL and d) normalized evolution associated spectra. The orange (A, EAS<sub>A</sub>) and green (B, EAS<sub>B</sub>) colored spectrum and decay profiles correspond to emission from the unrelaxed (Ex\*) and relaxed (Ex) excimer states.

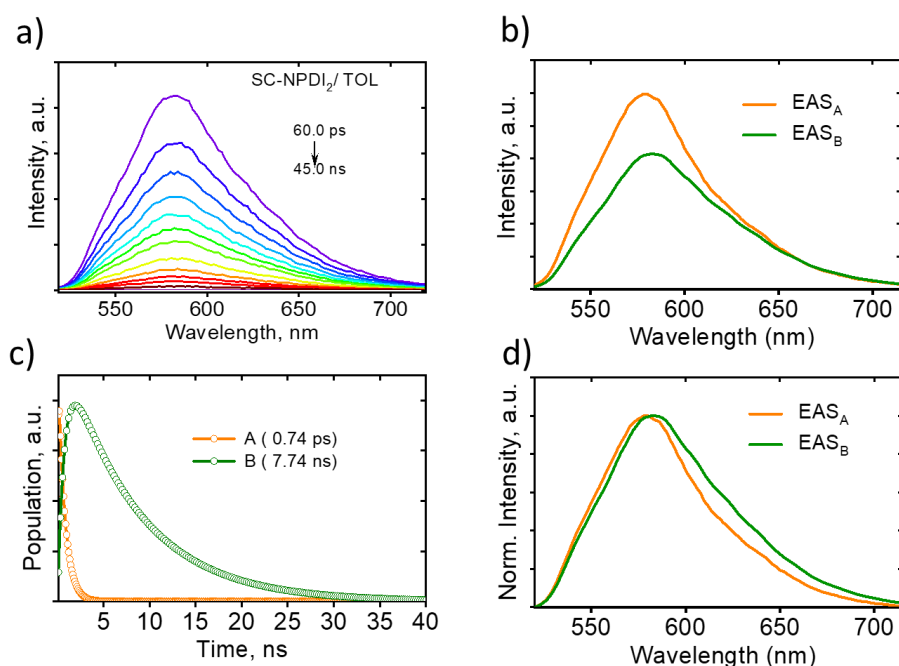


**Figure S8:** a) Time-resolved emission spectra (TRES,  $\lambda_{ex} = 478$  nm) of **SC-NPDI<sub>2</sub>** in TOL, b) Evolution associated spectra (EAS), (c) the relative population profiles of **SC-NPDI<sub>2</sub>** in TOL and d) normalized evolution associated spectra. The orange (A, EAS<sub>A</sub>) and green (B, EAS<sub>B</sub>) colored spectrum and decay profiles corresponds to emission from the unrelaxed (Ex\*) and relaxed (Ex) excimer states.

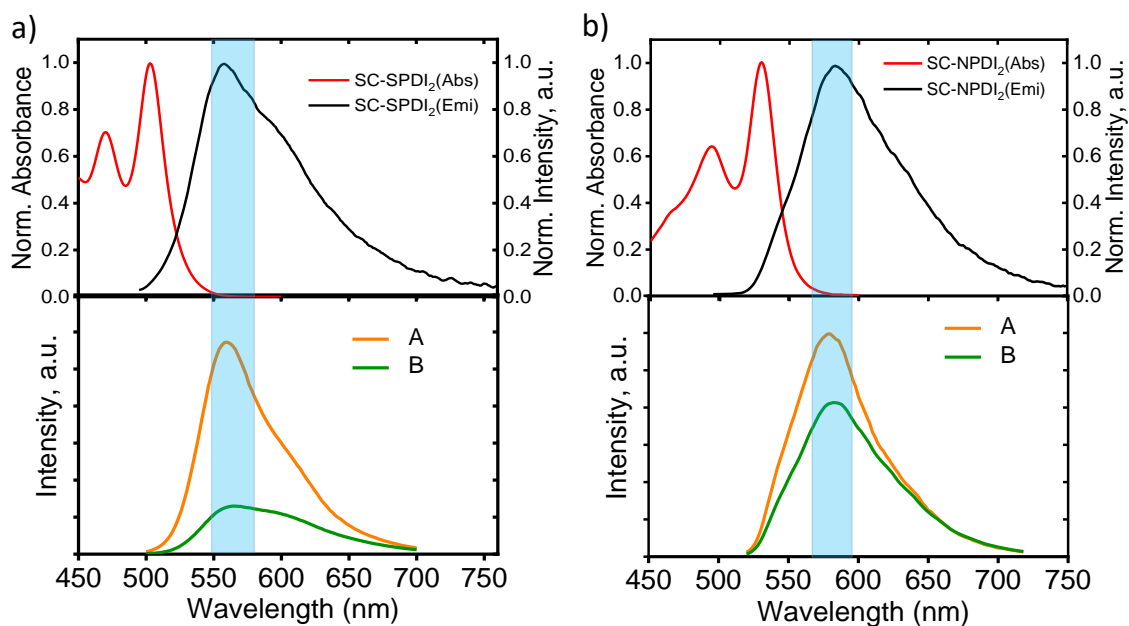


**Figure S9:** Comparison between the steady-state emission spectra (top) with the time-resolved emission spectra (bottom) of a) **SC-SPDI<sub>2</sub>** and b) **SC-NPDI<sub>2</sub>** recorded in TOL. The highlighted region in the spectra represents the emission maximum.

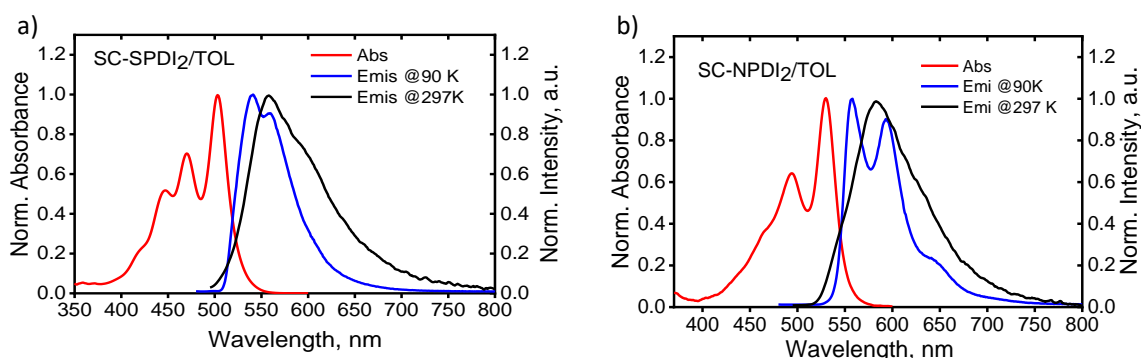


**Figure S10:** Steady-state UV-vis absorption spectra along with emission spectra (recorded at 90K and 297K) of a) **SC-SPDI<sub>2</sub>** and b) **SC-NPDI<sub>2</sub>** in TOL.

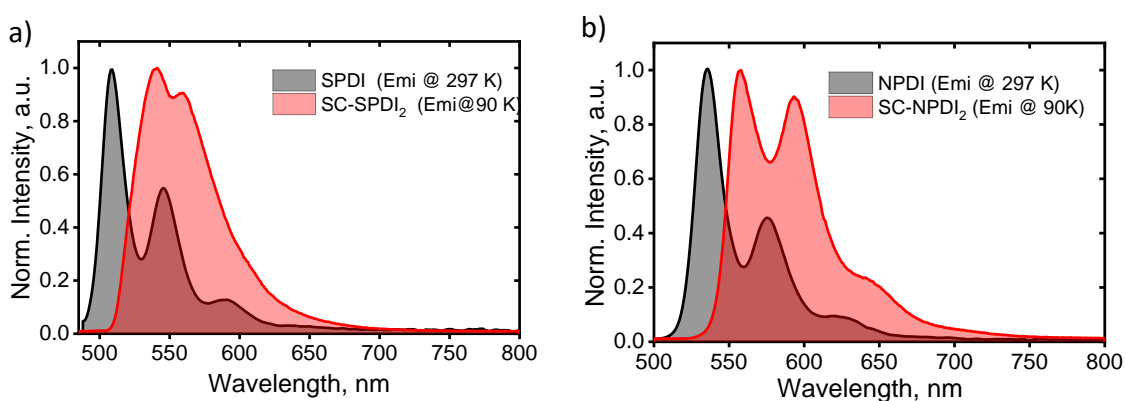


**Figure S11:** a) Emission spectra of **SPDI** at room temperature and **SC-SPDI<sub>2</sub>** at 90K and b) Emission spectra of **NPDI** at room temperature and **SC-NPDI<sub>2</sub>** at 90K in TOL.

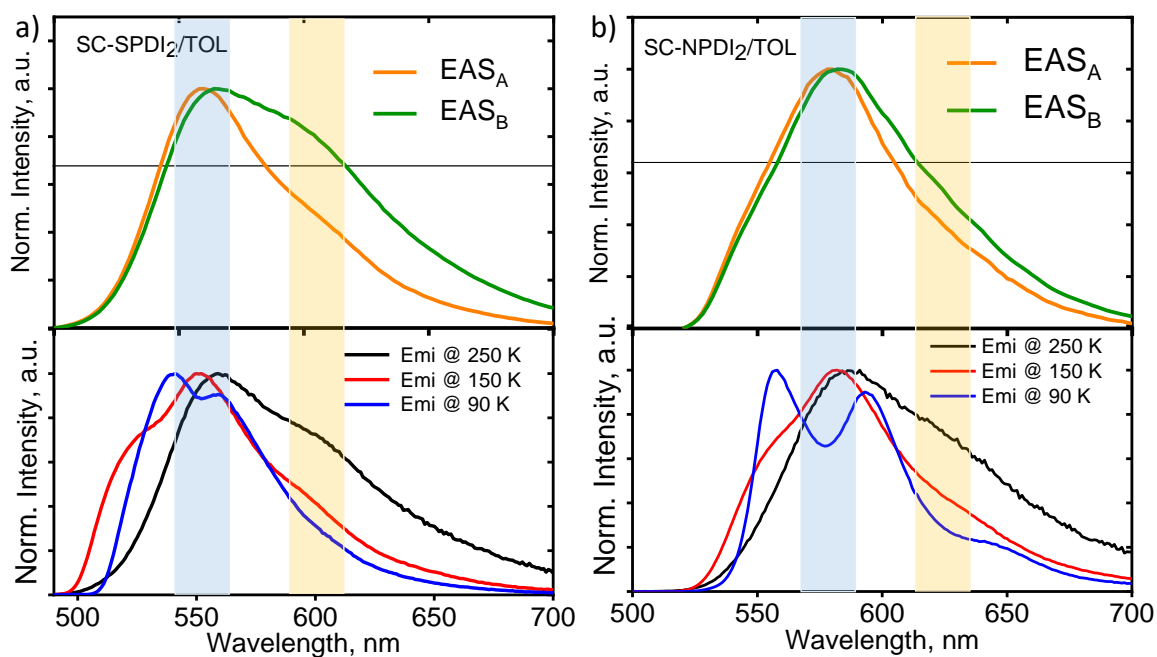


**Figure S12:** Comparison of time-resolved emission spectra with steady-state emission spectra at different temperatures for a) **SC-SPDI<sub>2</sub>** and b) **SC-NPDI<sub>2</sub>** in TOL.

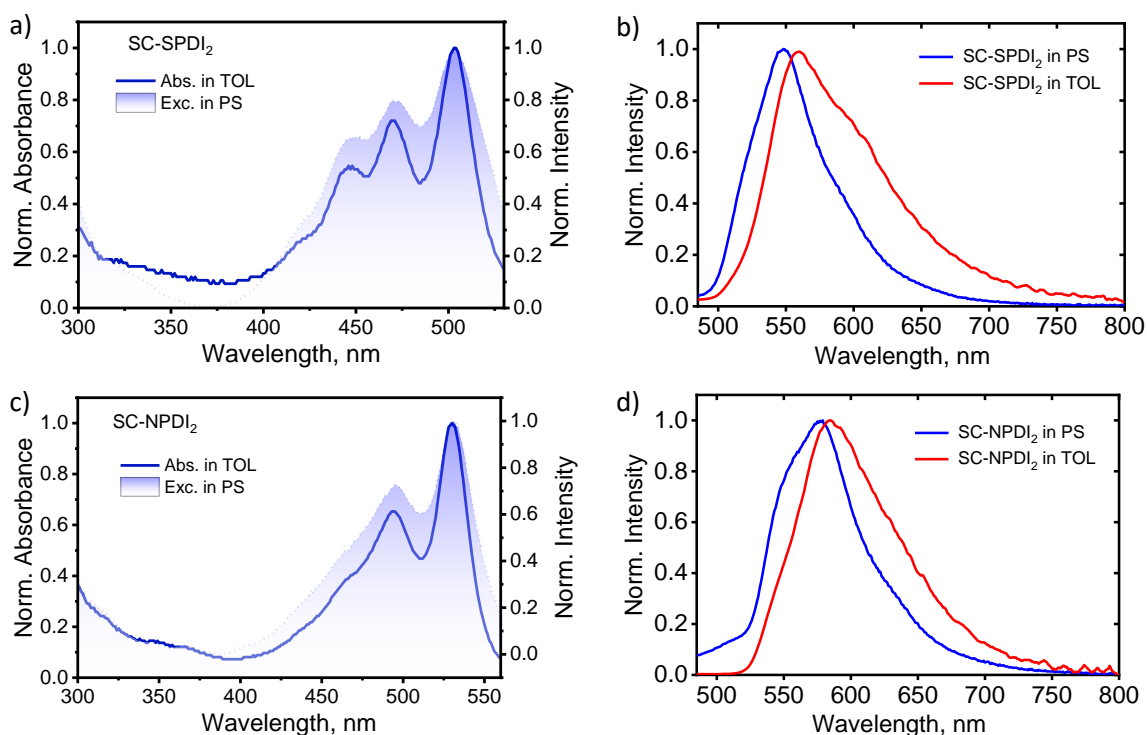


**Figure S13:** a) Absorption spectra and excitation spectra of **SC-SPDI<sub>2</sub>** in toluene and polystyrene matrix respectively, b) Emission spectra of **SC-SPDI<sub>2</sub>** in polystyrene matrix and toluene, c) Absorption spectra and excitation spectra of **SC-NPDI<sub>2</sub>** in toluene and polystyrene matrix respectively, d) Emission spectra of **SC-NPDI<sub>2</sub>** in polystyrene matrix and toluene

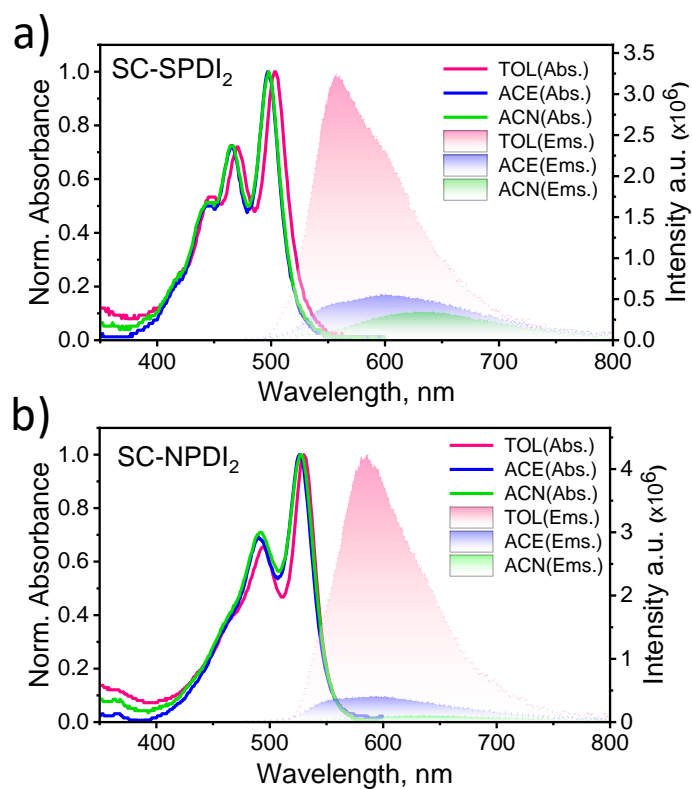


**Figure S14:** Solvent-dependent absorption and emission spectra of a) **SC-NPDI<sub>2</sub>** and b) **SC-SPDI<sub>2</sub>**.

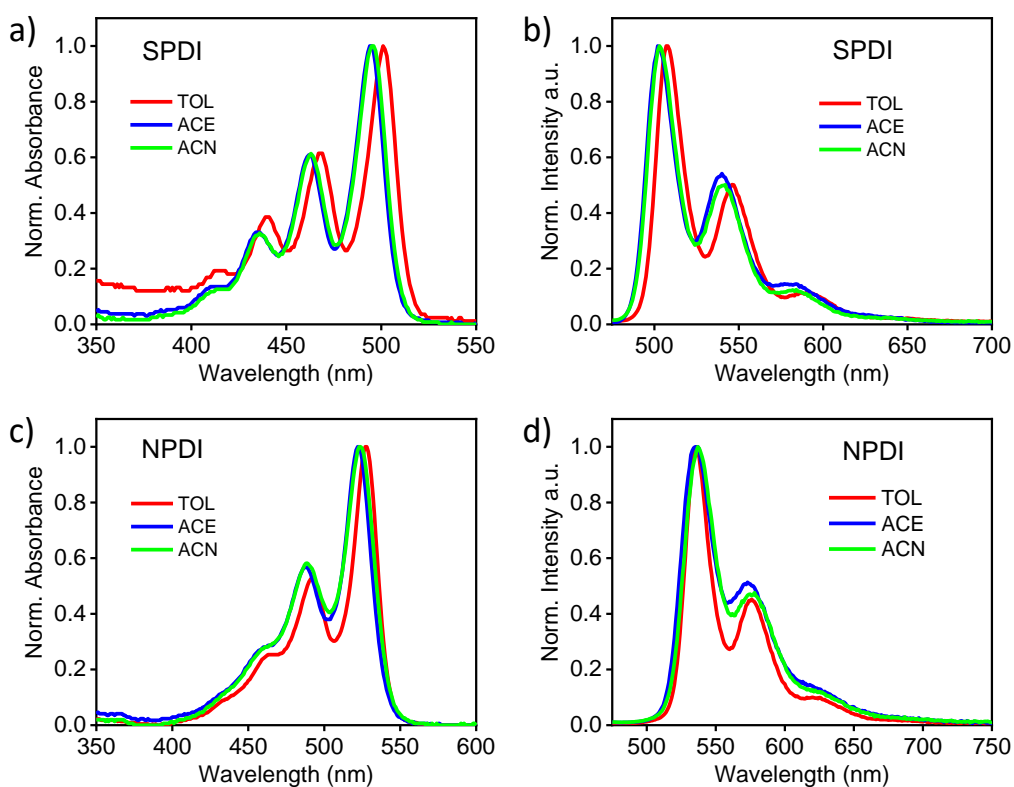


**Figure S15:** Normalised absorption and emission spectra of (a, b) **SPDI** and (c, d) **NPDI** in different solvents.

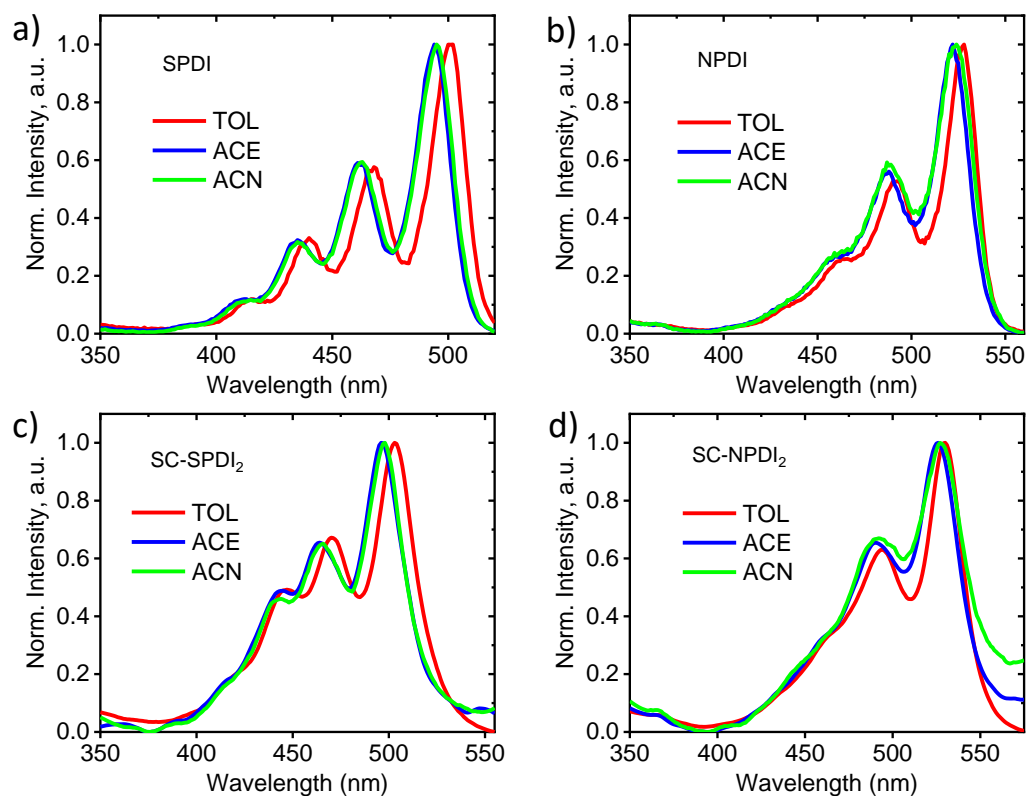


**Figure S16:** Normalised excitation spectra of a) **SPDI**, b) **NPDI**, c) **SC-SPDI<sub>2</sub>** and d) **SC-NPDI<sub>2</sub>** collected at emission maximum in different solvents.

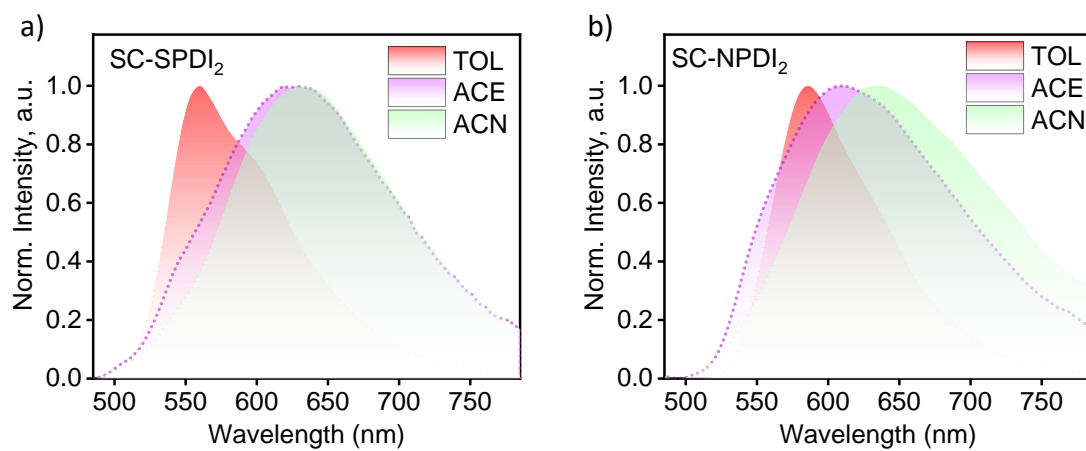


**Figure S17:** Solvent-dependent normalized emission spectra of a) **SC-SPDI<sub>2</sub>** and b) **SC-NPDI<sub>2</sub>**.

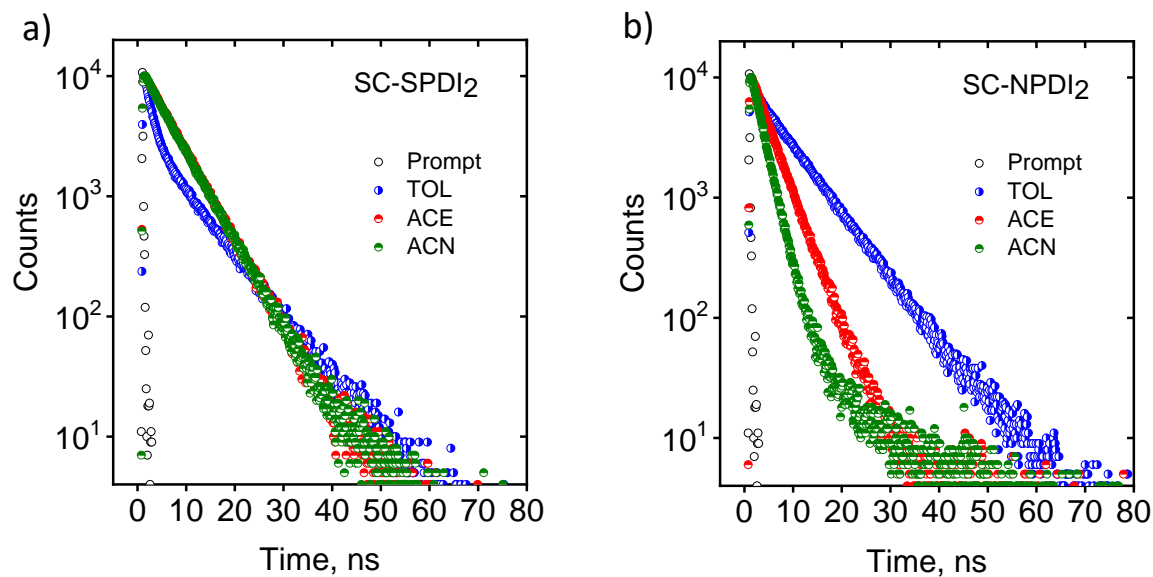


**Figure S18:** Fluorescence decay profiles of a) **SC-SPDI<sub>2</sub>** and b) **SC-NPDI<sub>2</sub>** in different solvents. The fluorescence decay profile of **SC-NPDI<sub>2</sub>** in ACN is biexponentially fitted. The second component is assigned to scattering contribution as **SC-NPDI<sub>2</sub>** has very low fluorescence quantum yield in ACN (<0.1%).

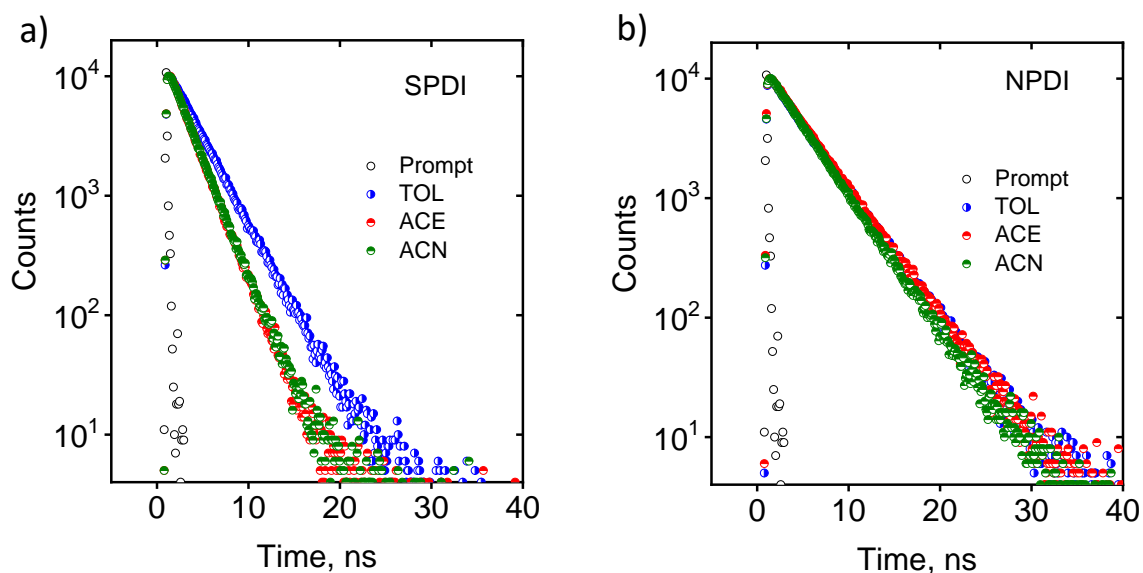


**Figure S19:** Fluorescence decay profiles of (a) **SPDI** and (b) **NPDI** in different solvents.

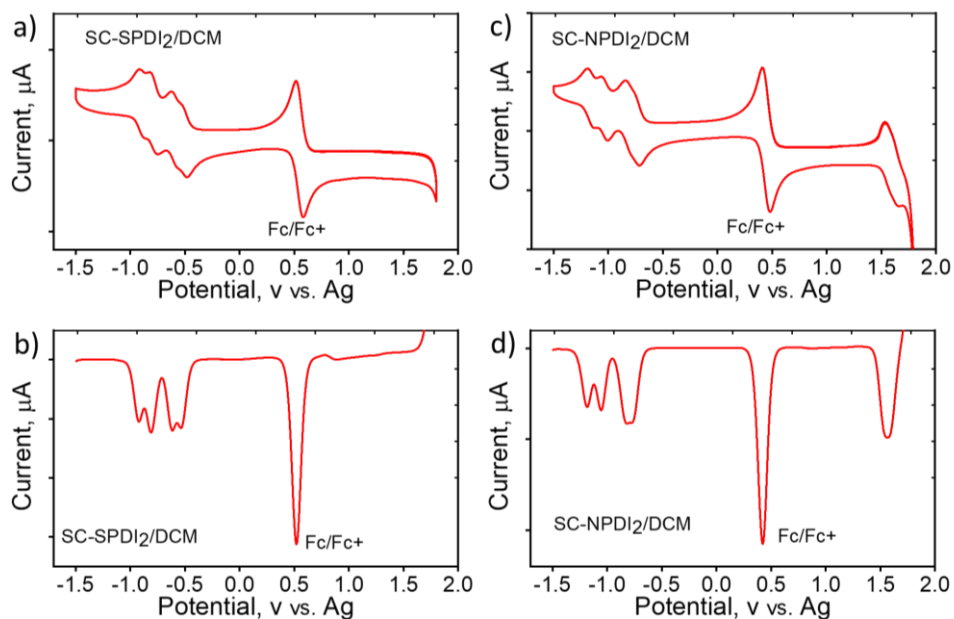


**Figure S20:** (a, c) Cyclic voltammetry data and (b, d) differential pulse voltammograms of **SC-SPDI<sub>2</sub>** and **SC-NPDI<sub>2</sub>** in CH<sub>2</sub>Cl<sub>2</sub>. (Tetrabutylammonium hexafluorophosphate (0.1 M) as the supporting electrolyte, scan rate 100 mV s<sup>-1</sup>. Fc/Fc+=ferrocene/ferrocenium couple).

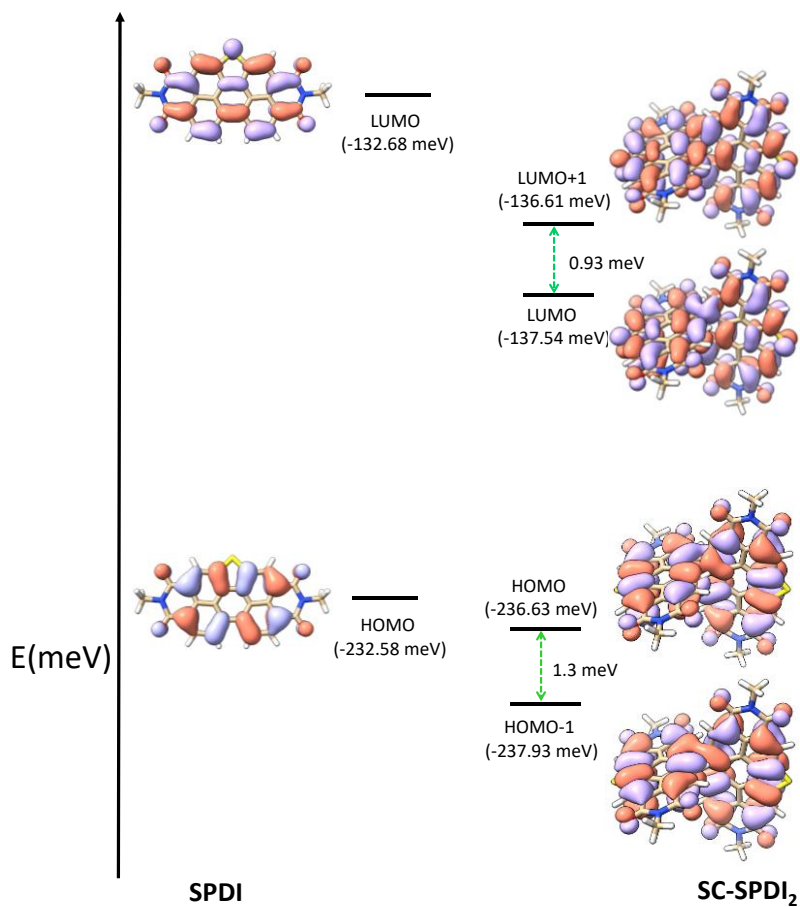


**Figure S21:** Energy level diagram with the frontier molecular orbitals of **SPDI** and **SC-SPDI<sub>2</sub>**.

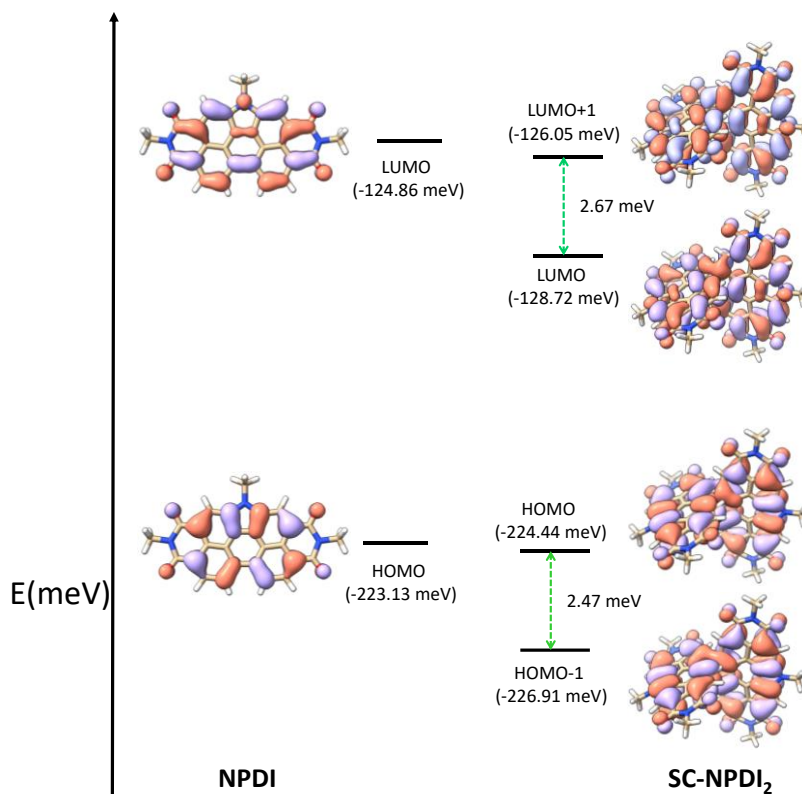


**Figure S22:** Energy level diagram with the frontier molecular orbitals of NPDI and SC-NPDI<sub>2</sub>.

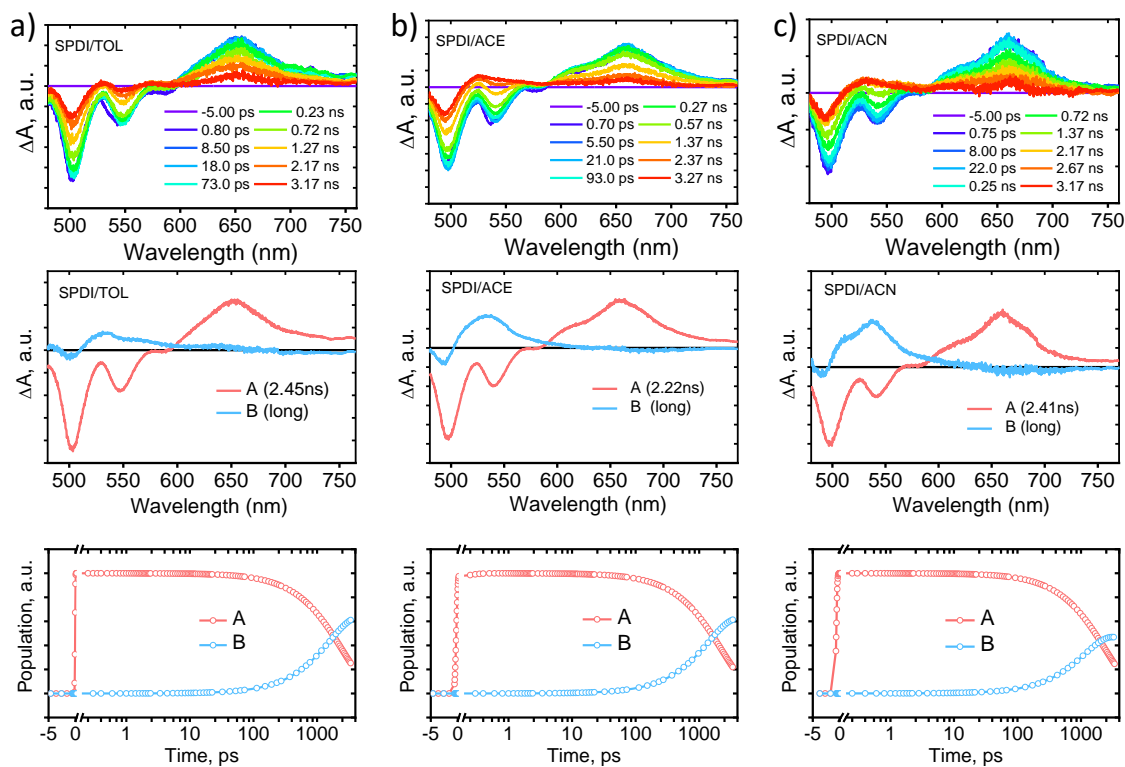


**Figure S23:** Femtosecond transient absorption spectra (top), evolution associated spectra (EAS, middle) and population profiles (bottom) of SPDI in different solvents.

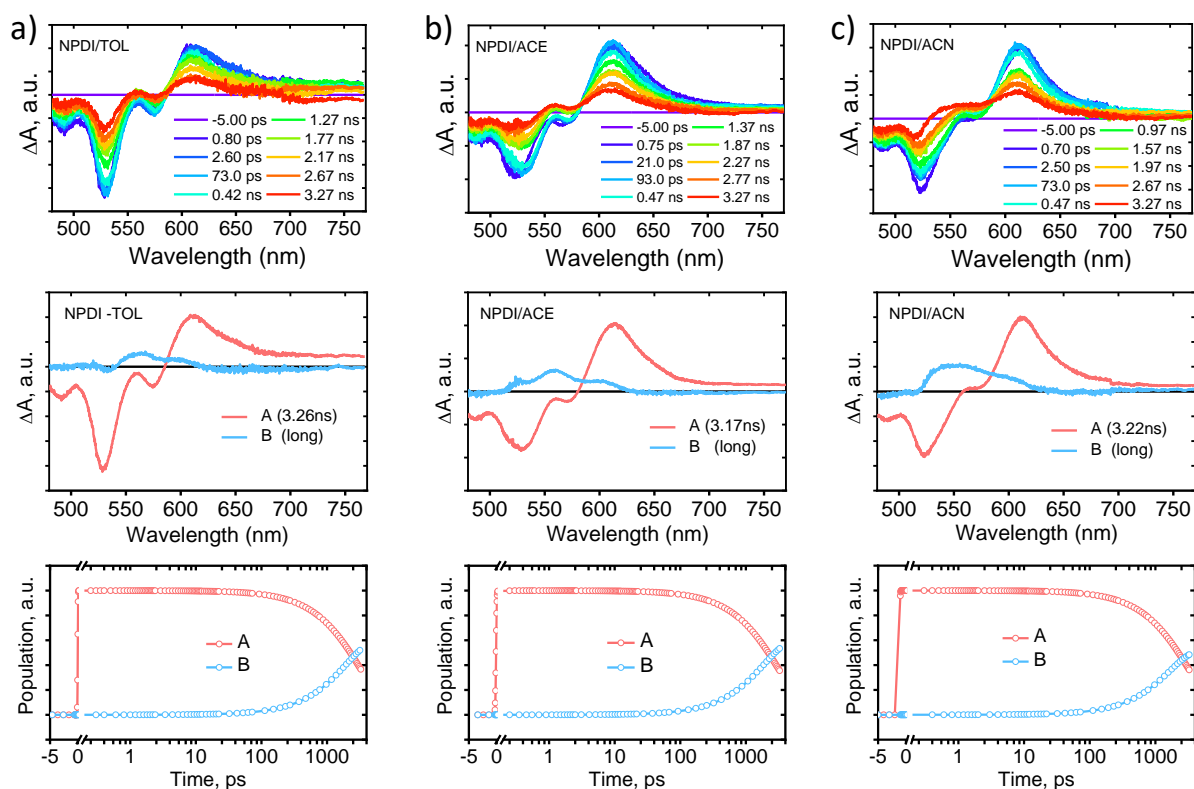


**Figure S24:** Femtosecond transient absorption spectra (top), evolution associated spectra (EAS, middle) and population profiles (bottom) of **NPD** in different solvents.

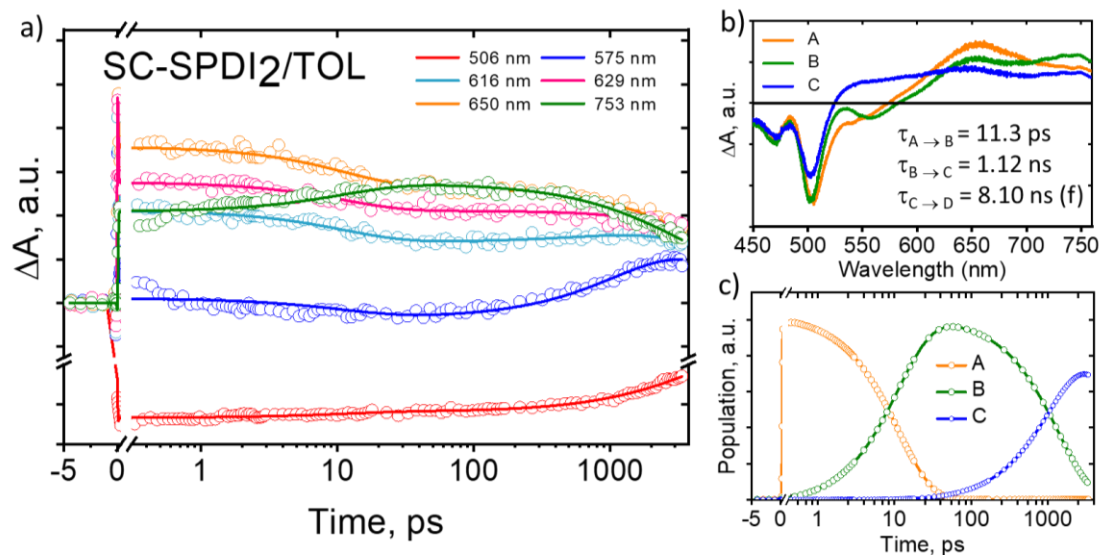


**Figure S25:** Global analysis fits for selected fsTA wavelengths of **SC-SPDI<sub>2</sub>** ( $\lambda_{\text{ex}} = 470$  nm) in toluene to A $\rightarrow$ B $\rightarrow$ C $\rightarrow$ D kinetic model. Fits are shown as solid lines. Evolution associated spectra (EAS, b) and population profiles (c) of **SC-SPDI<sub>2</sub>** in toluene.

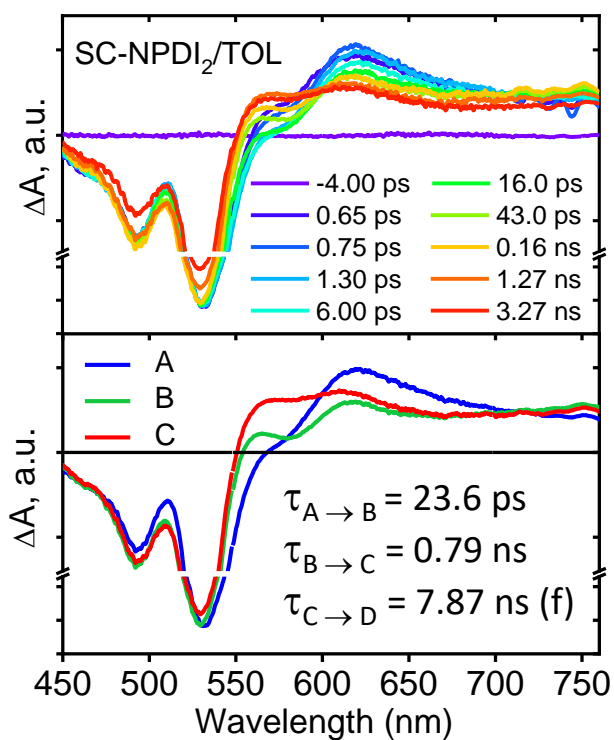


**Figure S26:** Femtosecond transient absorption spectra (top), Evolution associated spectra (bottom) of **SC-NPDI<sub>2</sub>** in toluene.

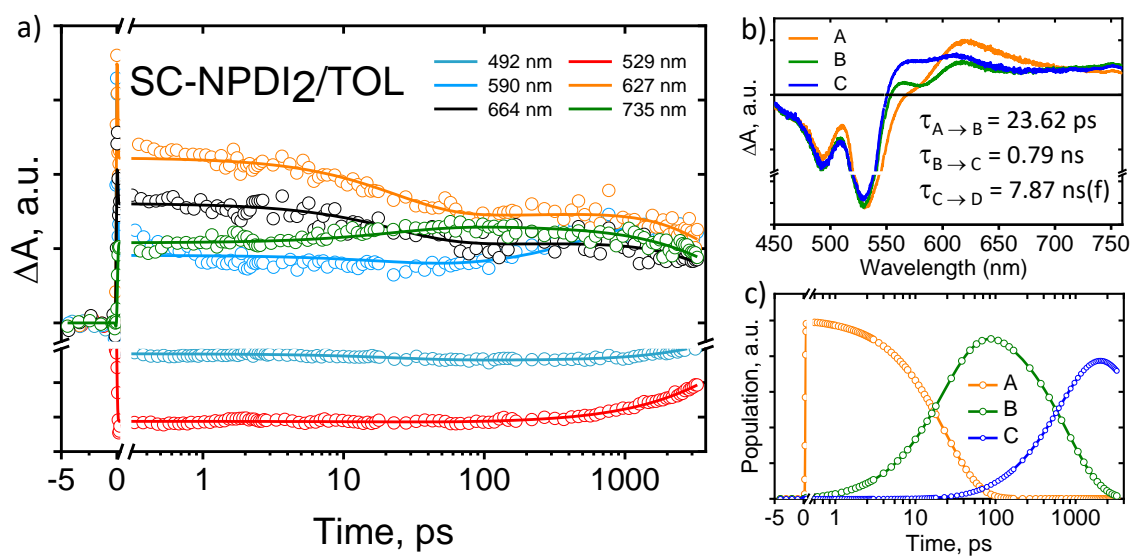


**Figure S27:** Global analysis fits for selected fsTA wavelengths of **SC-NPDI<sub>2</sub>** ( $\lambda_{ex} = 470$  nm) in toluene to A→B→C→D kinetic model. Fits are shown as solid lines. Evolution associated spectra (EAS, b) and population profiles (c) of **SC-NPDI<sub>2</sub>** in toluene.

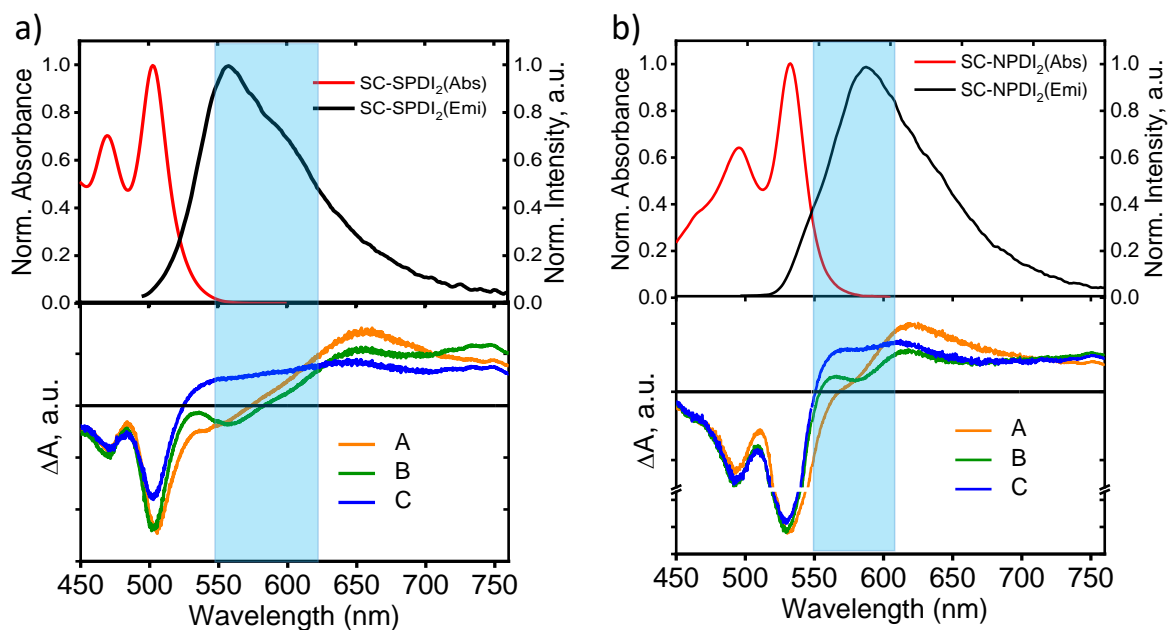


**Figure S28:** Comparison between the steady-state emission spectra (top) with the evolution associated spectra (bottom) of a) **SC-SPDI<sub>2</sub>** and b) **SC-NPDI<sub>2</sub>** recorded in TOL.

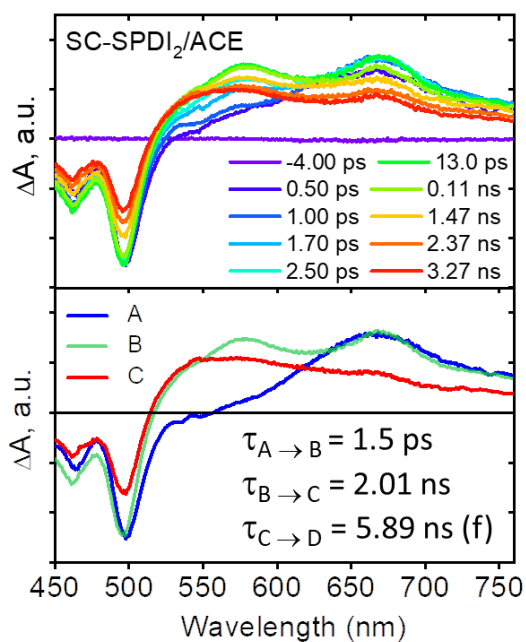


**Figure S29:** Femtosecond transient absorption spectra, Evolution associated spectra (EAS, bottom) of **SC-SPDI<sub>2</sub>** in acetone.

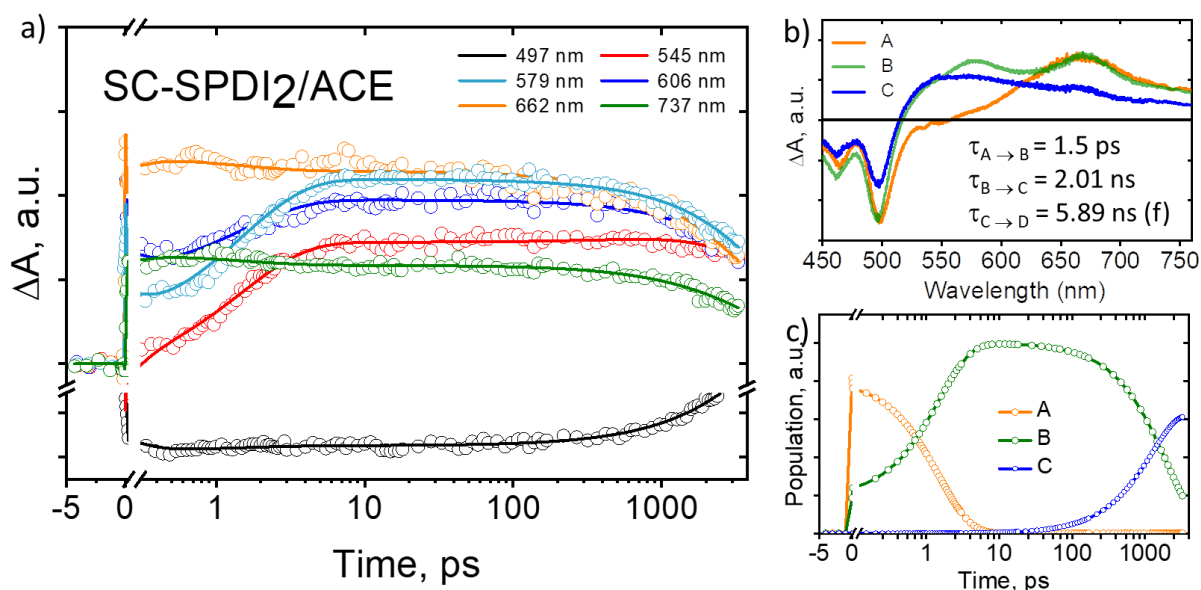


**Figure S30:** Global analysis fits for selected fsTA wavelengths of **SC-SPDI<sub>2</sub>** ( $\lambda_{ex} = 470$  nm) in acetone to A→B→C→D kinetic model. Fits are shown as solid lines. Evolution associated spectra (EAS, b) and population profiles (c) of **SC-SPDI<sub>2</sub>** in acetone.

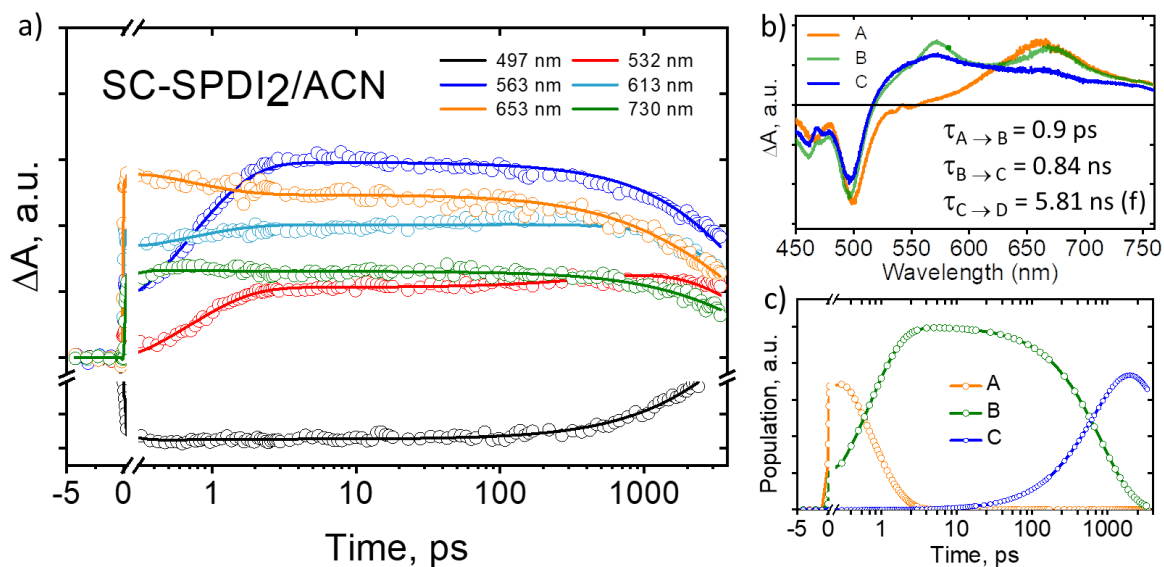


**Figure S31:** Global analysis fits for selected fsTA wavelengths of **SC-SPDI<sub>2</sub>** ( $\lambda_{ex} = 470$  nm) in acetonitrile to A→B→C→D kinetic model. Fits are shown as solid lines. Evolution associated spectra (EAS, b) and population profiles (c) of **SC-SPDI<sub>2</sub>** in acetonitrile.

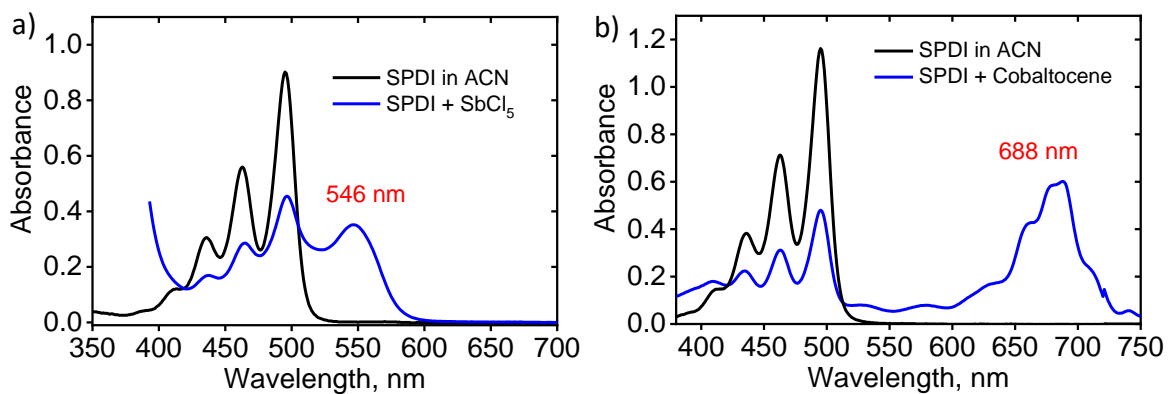


**Figure S32:** UV-vis absorption changes of **SPDI** in ACN upon the addition of a) antimony pentachloride ( $\text{SbCl}_5$ ) and b) cobaltocene ( $\text{CoCp}_2$ ).

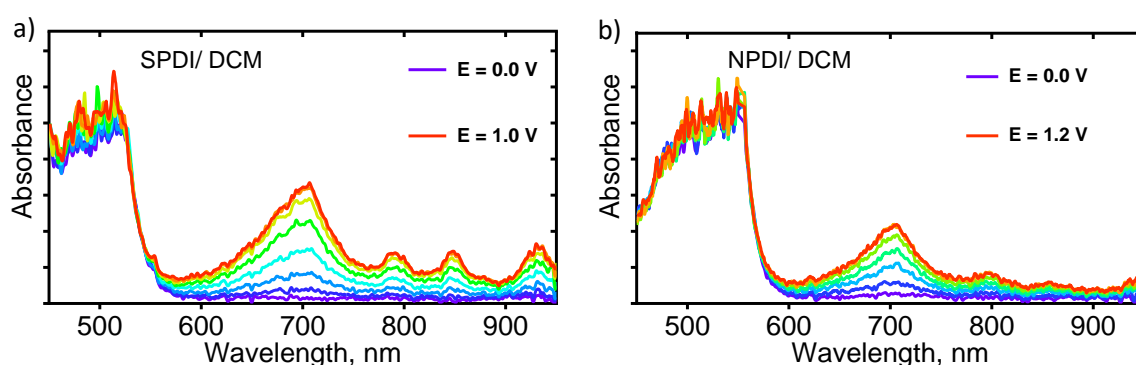


**Figure S33:** UV-Vis absorption spectra for the electrochemical reduction of a) **SPDI** and b) **NPDI**.

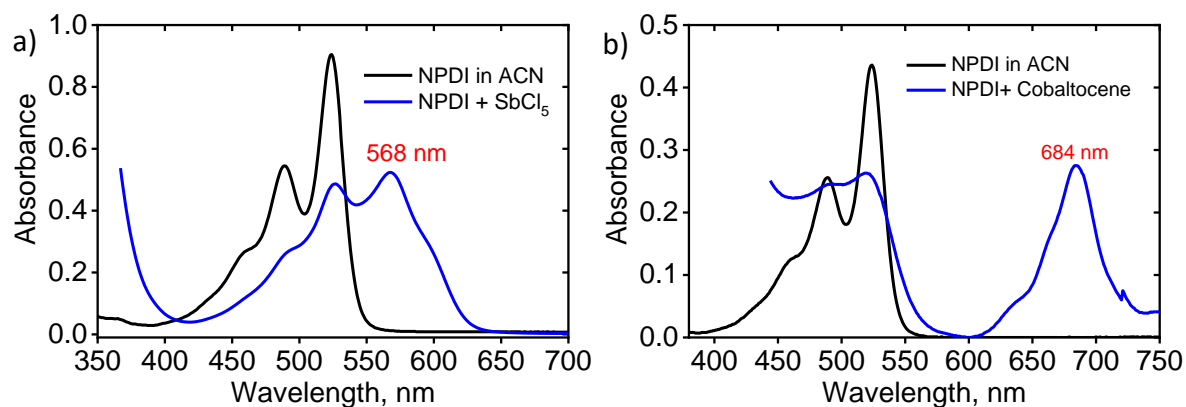


**Figure S34:** UV-vis absorption changes of **NPDI** in ACN upon the addition of a) antimony pentachloride ( $\text{SbCl}_5$ ) and b) cobaltocene ( $\text{CoCp}_2$ ).

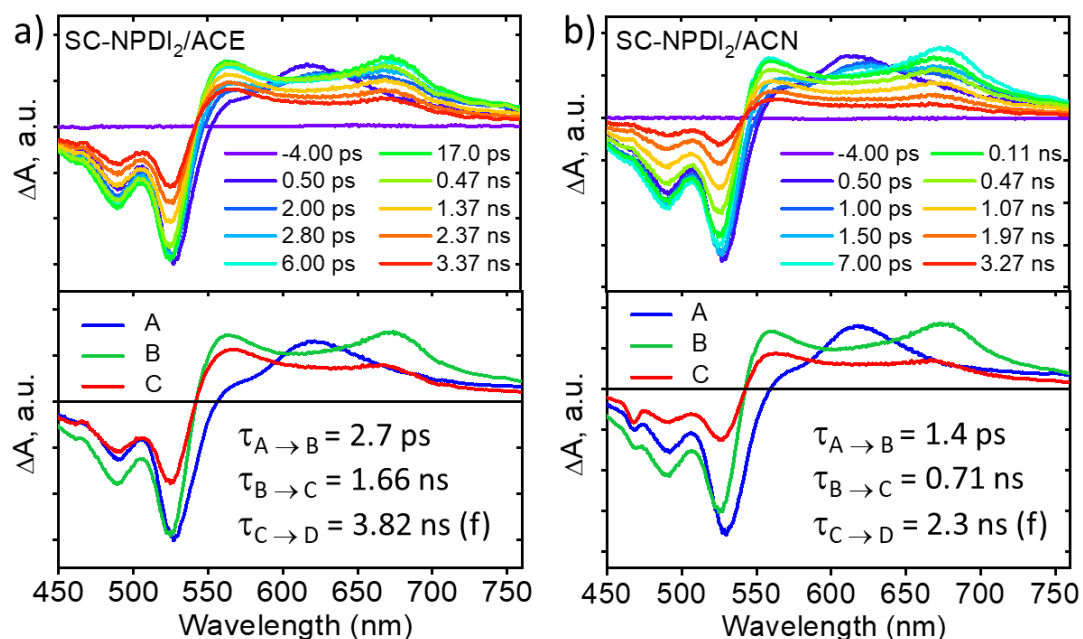


**Figure S35:** Femtosecond transient absorption spectra (top), Evolution associated spectra (EAS, bottom) of **SC-NPDI<sub>2</sub>** in a) acetone and b) acetonitrile.

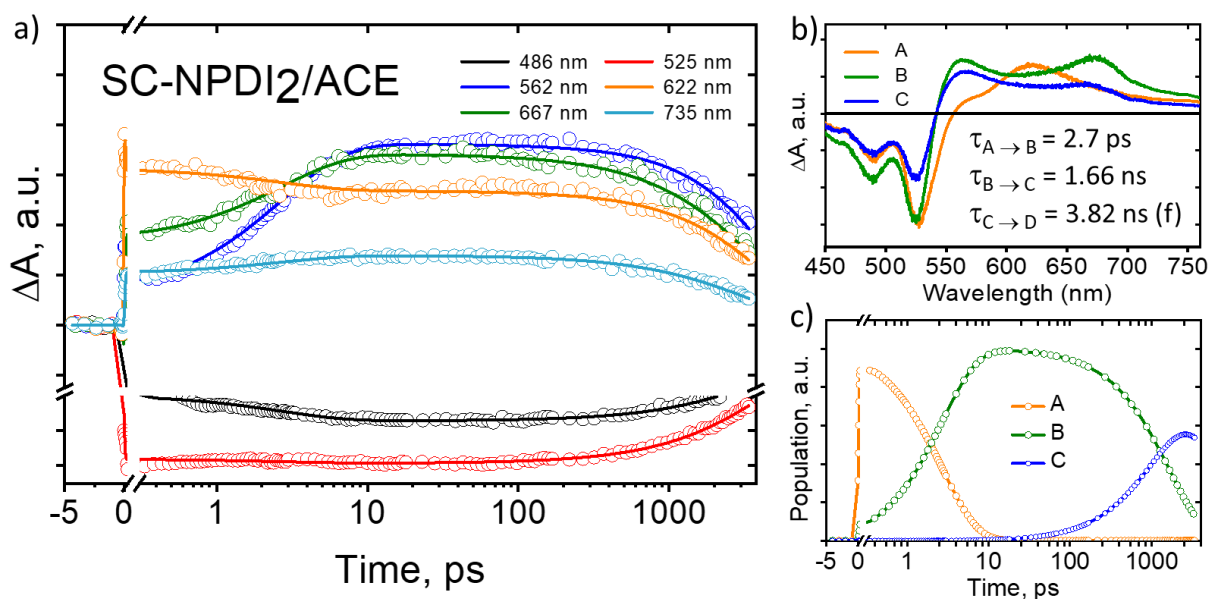


**Figure S36:** Global analysis fits for selected fsTA wavelengths of **SC-SPDI<sub>2</sub>** ( $\lambda_{ex} = 470$  nm) in acetone to A→B→C→D kinetic model. Fits are shown as solid lines. Evolution associated spectra (EAS, b) and population profiles (c) of **SC-NPDI<sub>2</sub>** in acetone.

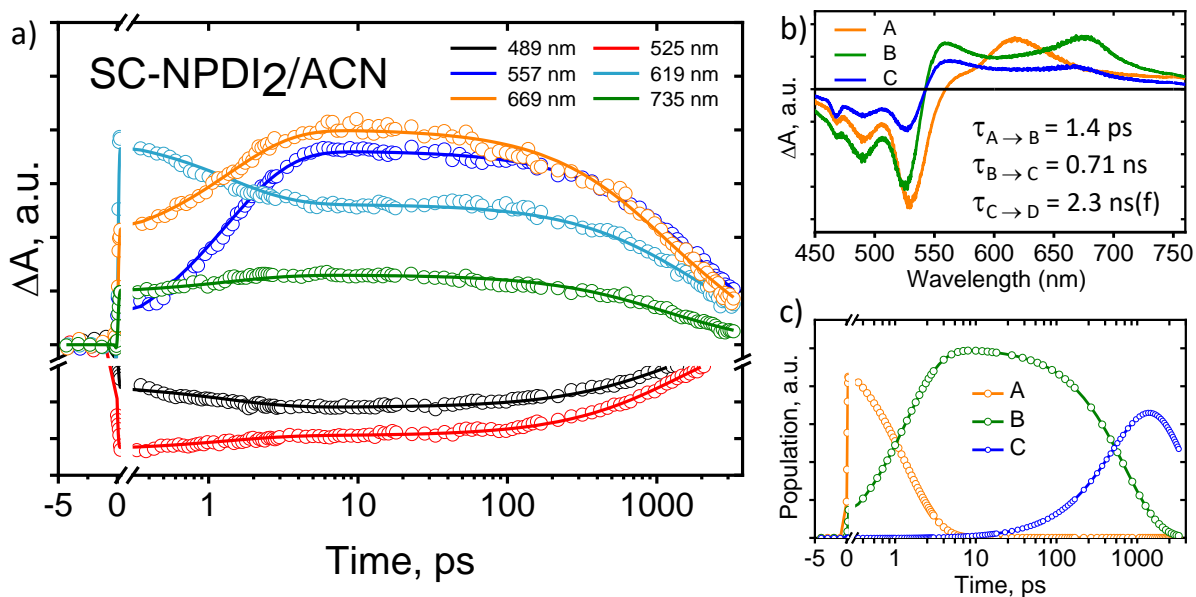


**Figure S37:** Global analysis fits for selected fsTA wavelengths of **SC-SPDI<sub>2</sub>** ( $\lambda_{ex} = 470$  nm) in acetone to A→B→C→D kinetic model. Fits are shown as solid lines. Evolution associated spectra (EAS, b) and population profiles (c) of **SC-NPDI<sub>2</sub>** in acetonitrile.

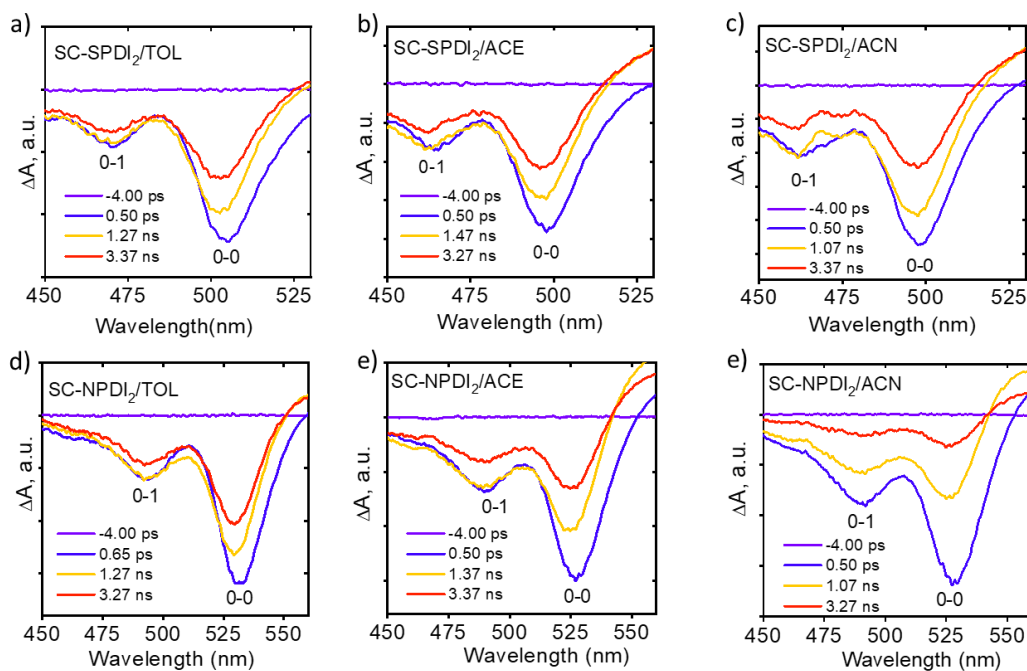


**Figure S38:** fsTA spectra highlighting the change in intensities of 0-0 and 0-1 vibronic bands for **SC-SPDI<sub>2</sub>** and **SC-NPDI<sub>2</sub>** in different solvents.

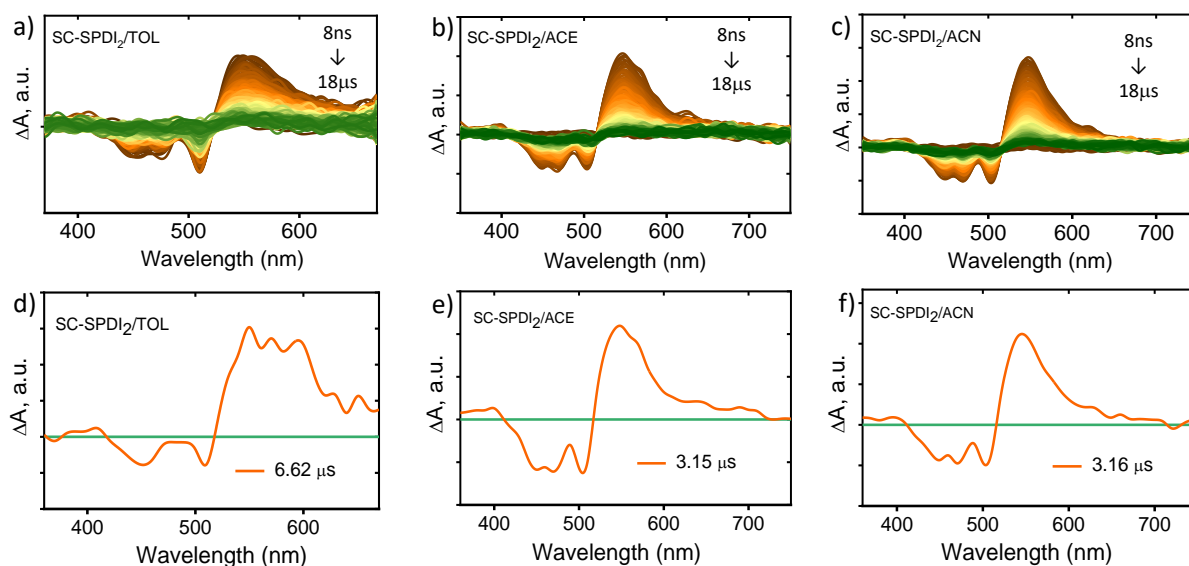


**Figure S39:** (Top) Nanosecond transient absorption spectra of **SC-SPDI<sub>2</sub>** in (a) TOL, (b) ACE and (c) ACN showing the excited-state dynamics after photoexcitation in N<sub>2</sub> atmosphere. (Bottom) Evolution associated spectra were reconstructed from global analysis of the A → GS model in all solvents.

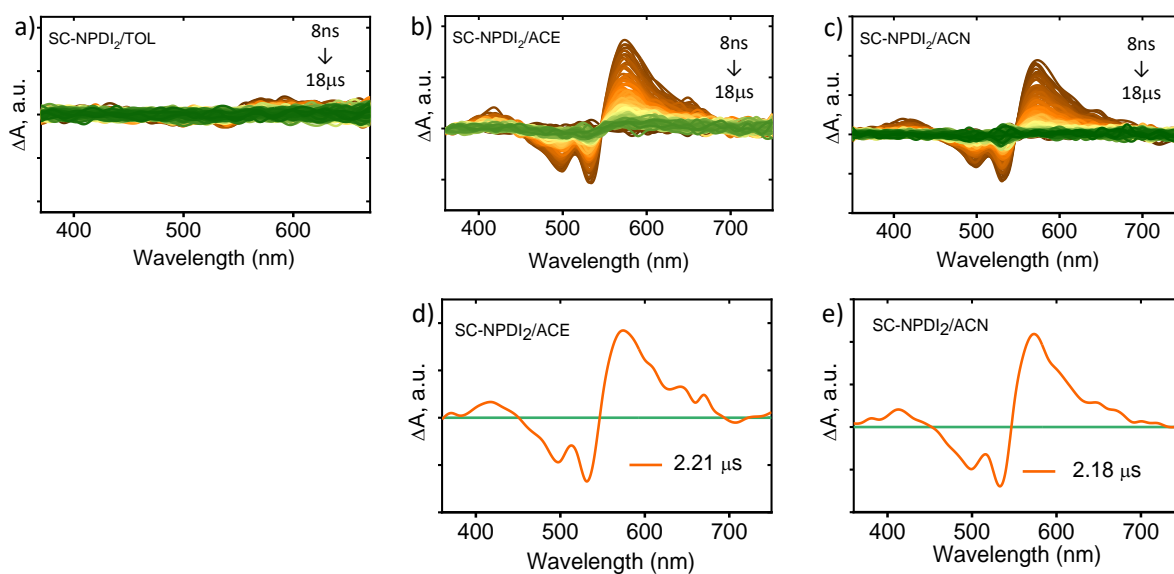


**Figure S40:** (Top) Nanosecond transient absorption spectra of **SC-NPDI<sub>2</sub>** in (a) TOL, (b) ACE and (c) ACN showing the excited-state dynamics after photoexcitation in N<sub>2</sub> atmosphere. (Bottom) Evolution associated spectra were reconstructed from global analysis of the A → GS model in all solvents.

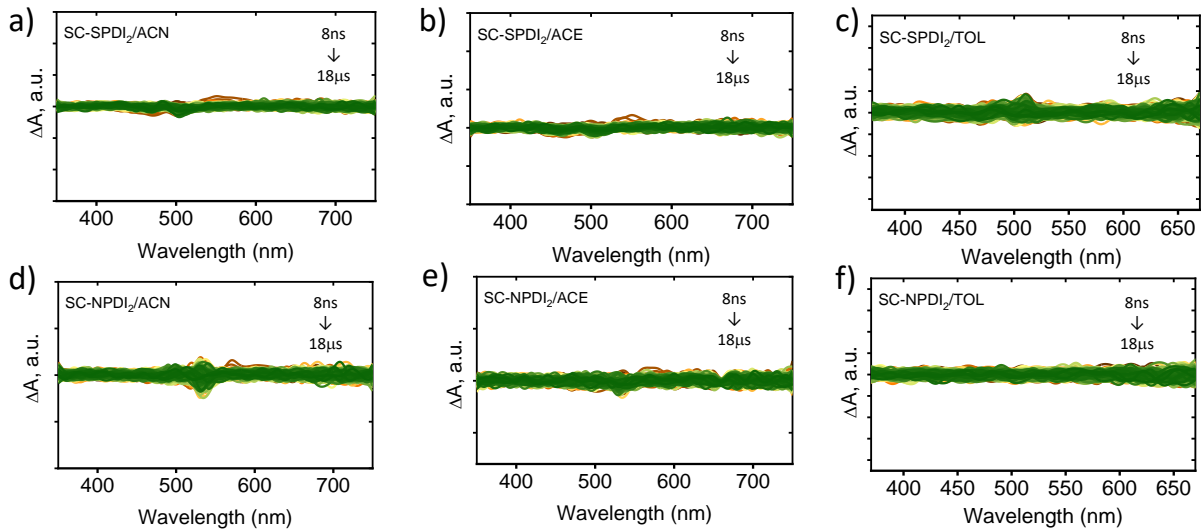


**Figure S41:** Nanosecond transient absorption spectra of **SC-SPDI<sub>2</sub>** in a) ACN, b) ACE, c) TOL and of **SC-NPDI<sub>2</sub>** in d) ACN, e) ACE, f) TOL after O<sub>2</sub> purging.

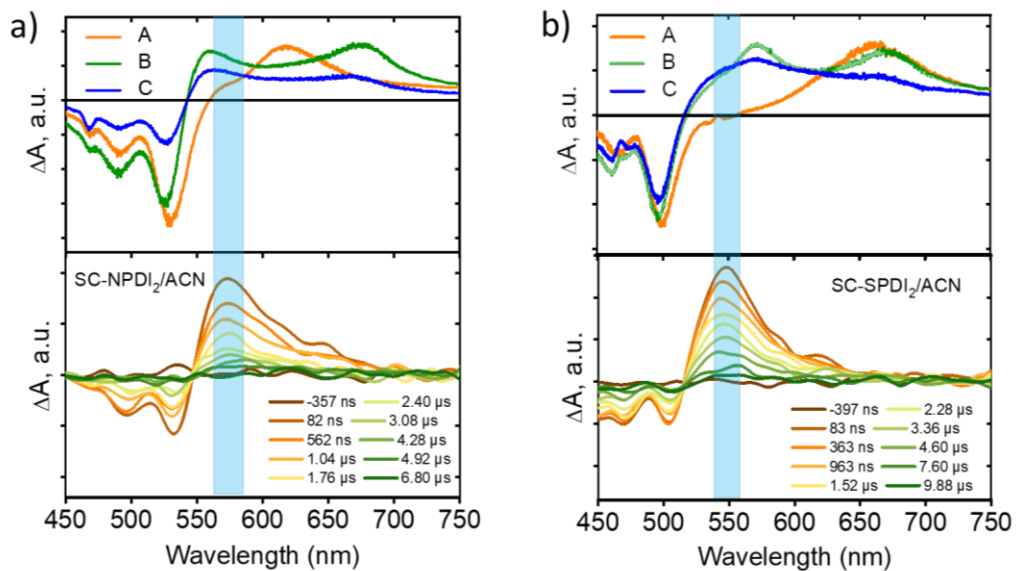


**Figure S42:** Comparison between the EAS from fsTA measurements (top) and nTA spectra (bottom) for a) **SC-NPDI<sub>2</sub>** and b) **SC-SPDI<sub>2</sub>**.

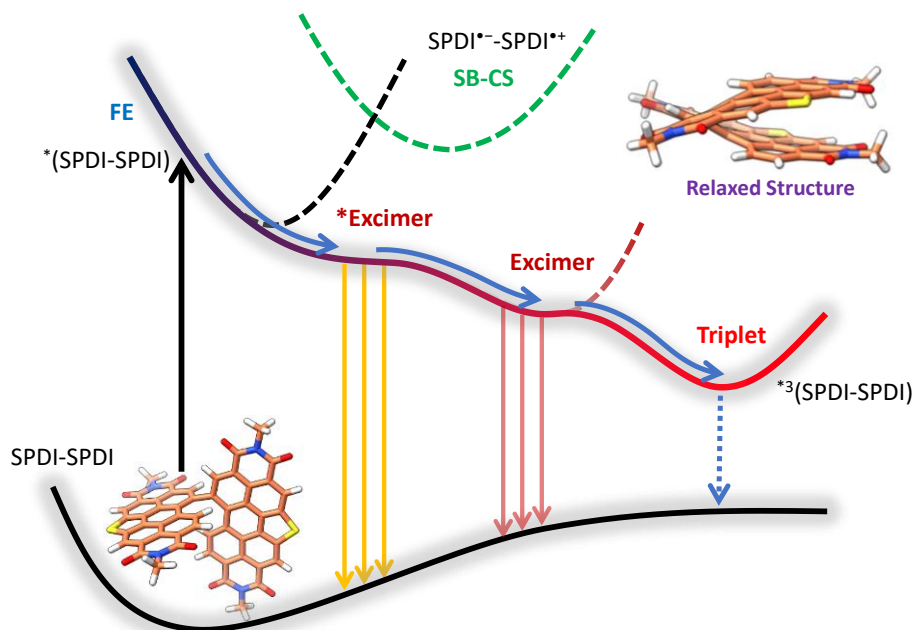


**Figure S43:** Schematic potential energy surface of **SC-SPDI<sub>2</sub>** in TOL summarising the excited state dynamics.

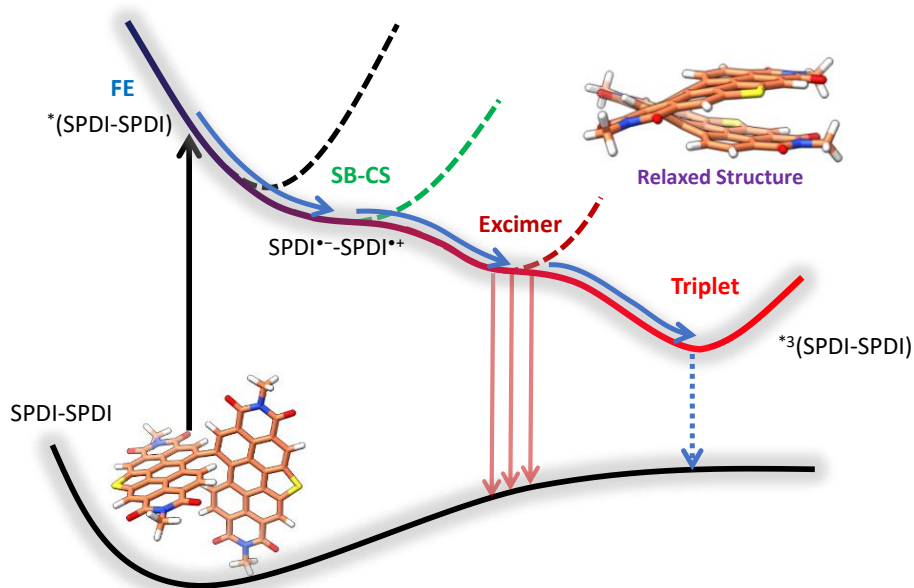


**Figure S44:** Schematic potential energy surface of **SC-SPDI<sub>2</sub>** in ACE and ACN summarising the excited state dynamics.

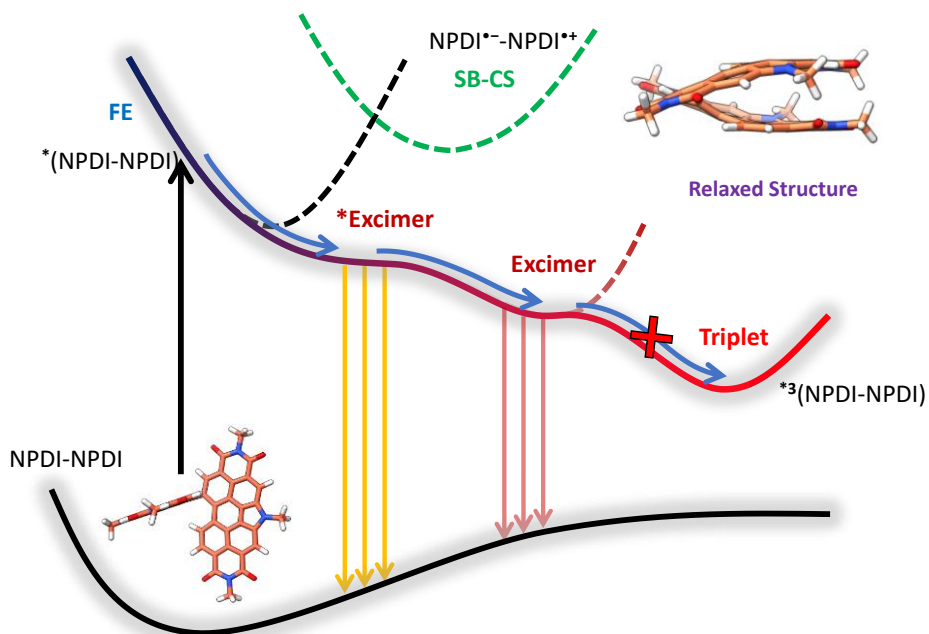


**Figure S45:** Schematic potential energy surface of **SC-NPDI<sub>2</sub>** in TOL summarising the excited state dynamics.

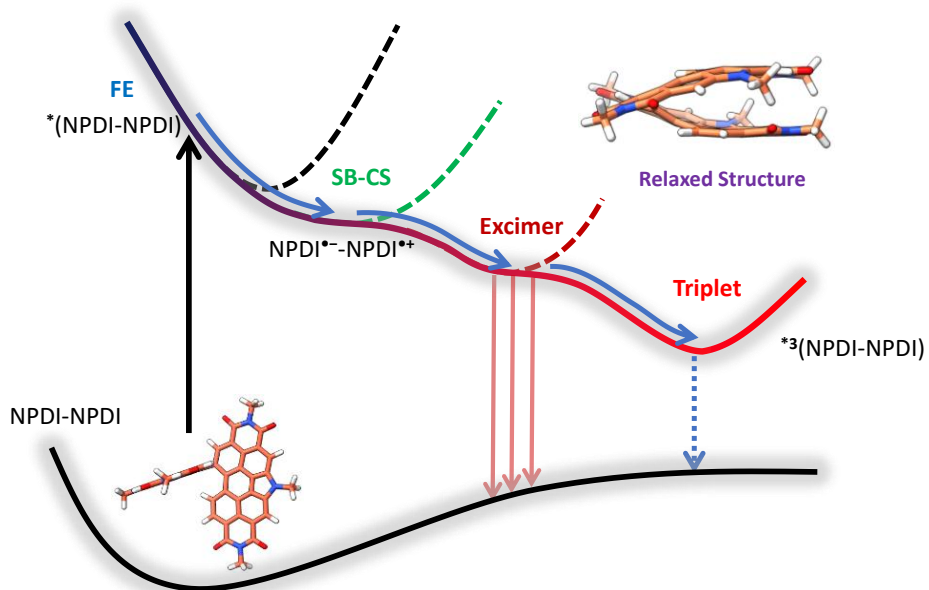


**Figure S46:** Schematic potential energy surface of **SC-NPDI<sub>2</sub>** in ACE and ACN summarising the excited state dynamics.

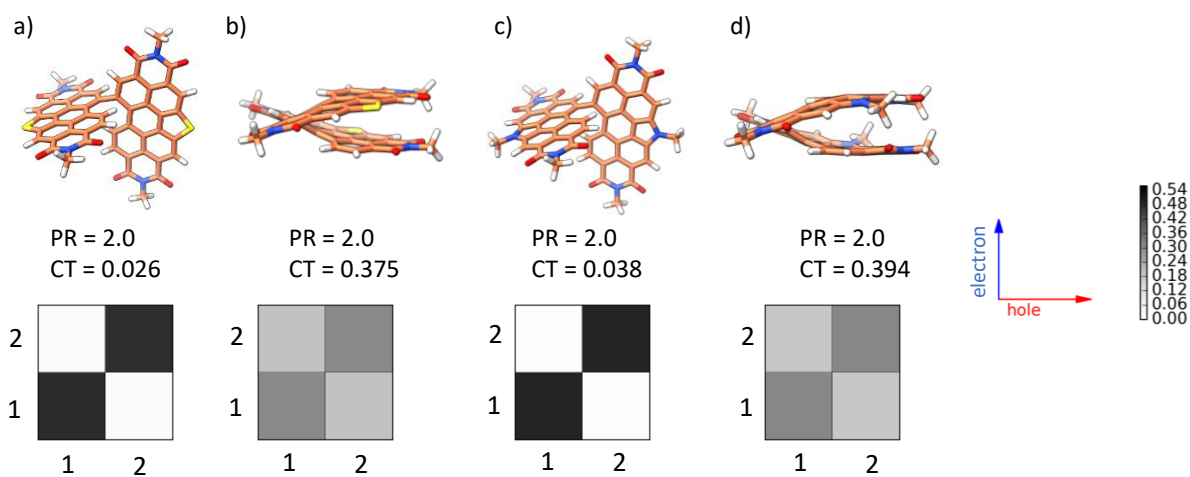


**Figure S47:** Molecular structures of the dimers and the corresponding PR and CT values for the transition to the first singlet excited state along with the electron-hole correlation plots (a,b) SC-SPDI<sub>2</sub> and (c,d) SC-NPDI<sub>2</sub>.

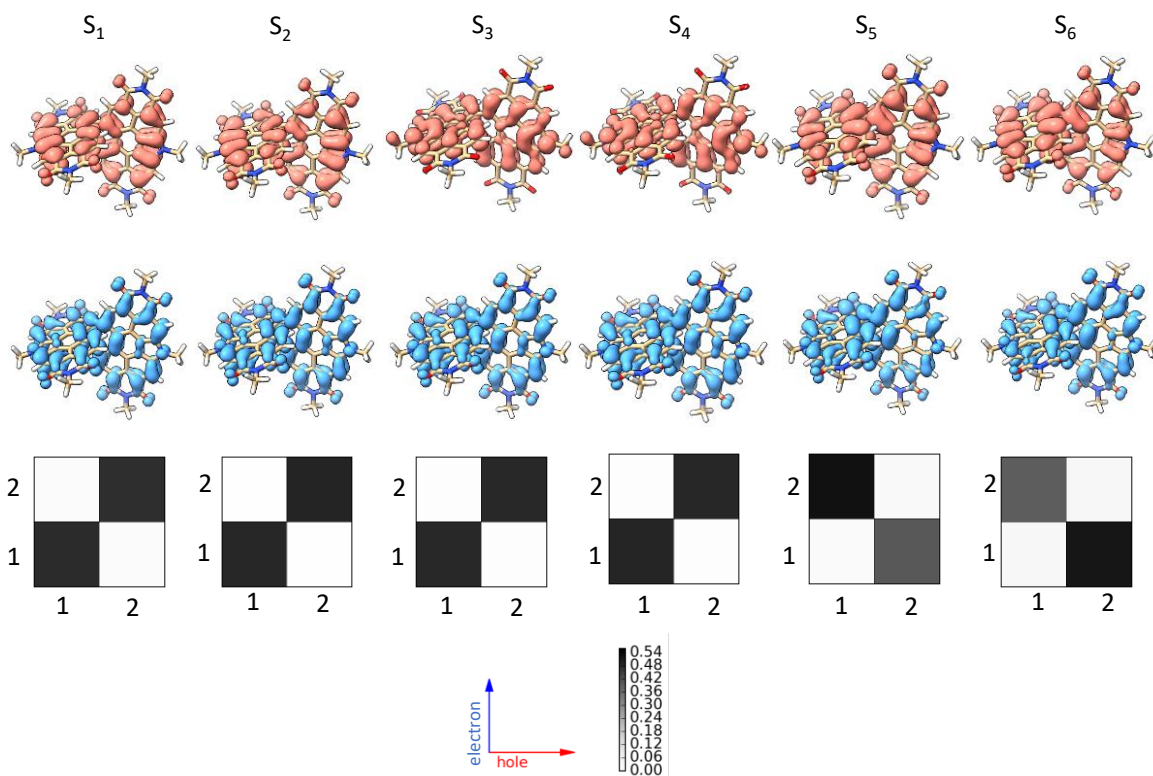


**Figure S48:** Hole and electron isosurfaces for the first six singlet excited state transitions and the corresponding electron-hole correlation plots of SC-NPDI<sub>2</sub> in the near-orthogonal geometry.

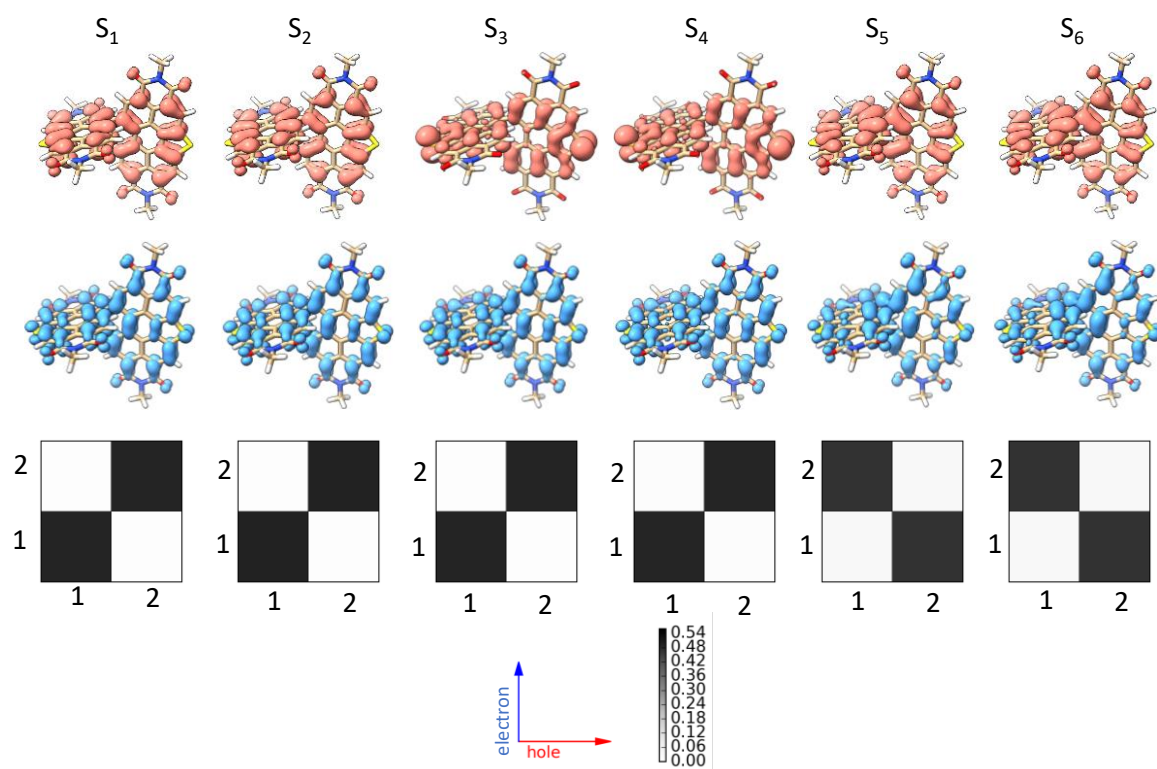


**Figure S49:** Hole and electron isosurfaces for the first six singlet excited state transitions along with the corresponding electron-hole correlation plots of **SC-SPDI<sub>2</sub>** in the near-orthogonal geometry.

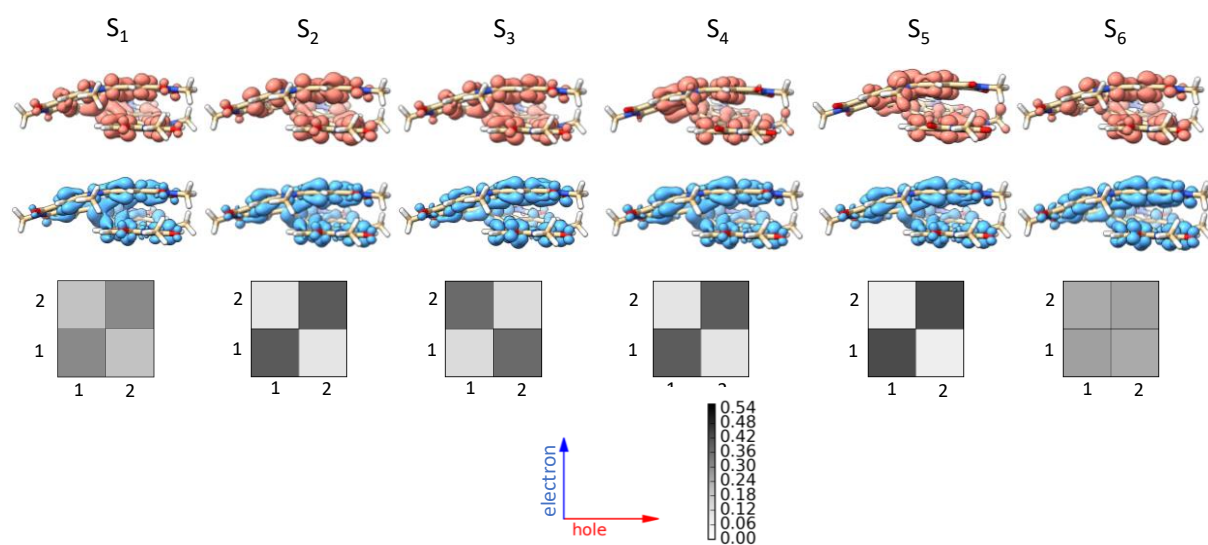


**Figure S50:** Hole and electron isosurfaces for the first six singlet excited state transitions along with the corresponding electron-hole correlation plots of **SC-NPDI<sub>2</sub>** in the foldamer geometry.

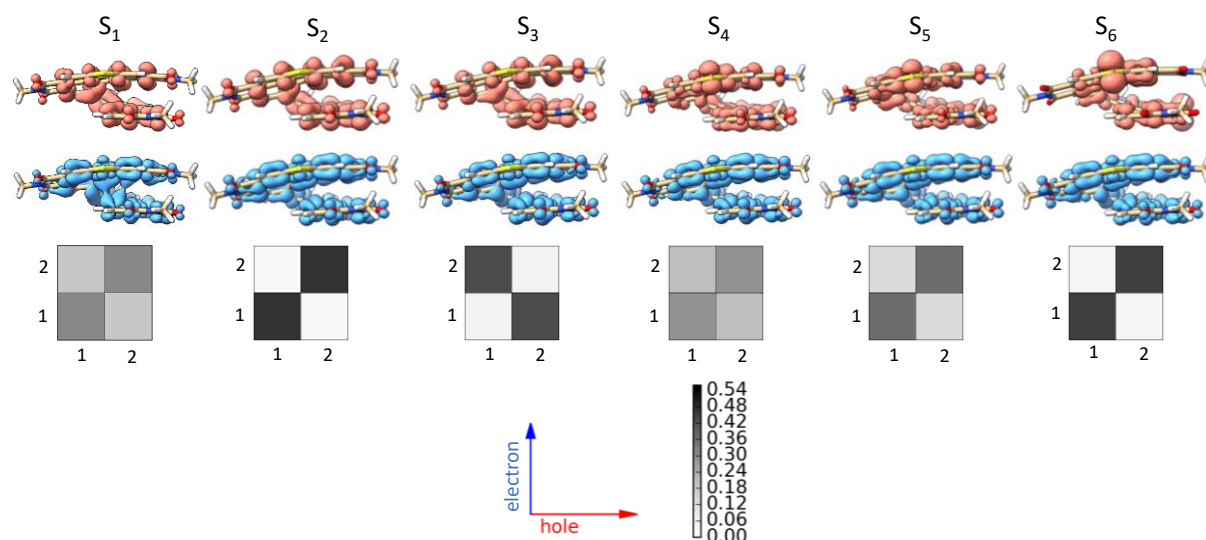


**Figure S51:** Hole and electron isosurfaces for the first six singlet excited state transitions along with the corresponding electron-hole correlation plots of **SC-SPDI<sub>2</sub>** in the foldamer geometry.

## References

- (1) Citation | Gaussian.com <https://gaussian.com/citation/> (accessed Jun 3, 2021).
- (2) Lu, T.; Chen, F. Multiwfn: A Multifunctional Wavefunction Analyzer. *J. Comput. Chem.* 2012, 33, 580–592.
- (3) Snellenburg, J. J.; Laptinok, S.; Seger, R.; Mullen, K. M.; van Stokkum, I. H. M. Glotaran: A Java-Based Graphical User Interface for the R Package TIMP. *J. Stat. Softw.* 2012, 49, 1–22.
- (4) Deng, P.; Liu, L.; Ren, S.; Li, H.; Zhang, Q. N-Acylation: An Effective Method for Reducing the LUMO Energy Levels of Conjugated Polymers Containing Five-Membered Lactam Units. *Chem. Commun.* 2012, 48, 6960–6962. SI 28
- (5) Li, G.; Yang, W.; Wang, S.; Liu, T.; Yan, C.; Zhang, Y.; Li, D.; Wang, X.; Hao, P.; Li, J.; Huo, L.; Yan, He.; Tang, B. Methane-perylene diimide-based small molecule acceptors for high efficiency non-fullerene organic solar cells. *J. Mater. Chem. C*, 2019, 7, 10901-10907
- (6) Weller, A. Photoinduced Electron Transfer in Solution: Exciplex and Radical Ion Pair Formation Free Enthalpies and Their Solvent Dependence. *Z. Phys. Chem.* 1982, 133, 93–98.
- (7) Wu, Y. L.; Brown, K. E.; Wasielewski, M. R. Extending Photoinduced Charge Separation Lifetimes by Using Supramolecular Design: Guanine-Perylenediimide G-Quadruplex. *J. Am. Chem. Soc.* 2013, 135, 13322–13325.
- (8) Plasser, F. TheoDORE: A Toolbox for a Detailed and Automated Analysis of Electronic Excited State Computations. *J. Chem. Phys.* 2020, 152, 084108.
- (9) Plasser, F.; Lischka, H. Analysis of Excitonic and Charge Transfer Interactions from Quantum Chemical Calculations. *J. Chem. Theory Comput.* 2012, 8, 2777–2789.
- (10) Hendsbee, A. D.; Sun, J.-P.; Law, W. K.; Yan, H.; Hill, I. G.; Spasyuk, D. M.; Welch, G. C. Synthesis, Self-Assembly, and Solar Cell Performance of N-Annulated Perylene Diimide Non-Fullerene Acceptors. *Chem. Mater.* 2016, 28, 19, 7098–7109
- (11) Meng, D.; Sun, D.; Zhong, C.; Liu, T.; Fan, B.; Huo, L.; Li, Y.; Jiang, W.; Choi, H.; Kim, T.; Kim, J. Y.; Sun, Y.; Wang, Z.; Heeger, A. J. High-Performance Solution-Processed Non-Fullerene Organic Solar Cells Based on Selenophene-Containing Perylene Bisimide Acceptor. *J. Am. Chem. Soc.* 2016, 138, 375–380